Optimization of proton therapy plans with respect to biological and physical dose distributions

Helge Henjum

Supervisors: Kristian S. Ytre-Hauge, Tordis J. Dahle and Eivind Rørvik

Master Thesis in Medical Physics and Technology

Department of Physics and Technology

University of Bergen

June 2018

Acknowledgements

First of all I would like to thank my supervisors Dr. Kristian S. Ytre-Hauge, and Ph.D. candidates Eivind Rørvik and Tordis J. Dahle. Your help, guidance and dedication have been invaluable.

Thank you Kristian, for introducing me to the interesting field of proton therapy, and excellent guidance and feedback throughout this project. Thank you Tordis, for helping and guiding and helping me with the optimizer, and for the thorough proofreading the document several times. Thank you Eivind, for the help with all the different aspects of FLUKA and reading through my thesis on different occasions. I will also thank Ph.D candidate Lars Fredrik Fjæra, for proofreading and helping me with the dose verification scripts and creating the Eclipse treatment plans.

Thanks to the people at room 534, for good companionship the last two years, and especially Viljar for many coffee-breaks and lively discussions. I would also like to thank the classmates, Anders, Daniel, Håkon, Karl, Magnus and Viljar, that began with me five years ago. You have made the past five years into a fun and exciting journey.

I will also thank my family for their positivity and encouragement during this project. Finally, I would like to thank Malin for the enormous love and support you have shown during this period, it has meant a lot to me.

Bergen, June 2018

Helge Henjum

Abstract

Introduction: Proton therapy is a radiation treatment method growing around the world. This is mainly due to the protons ability to deposit dose more conformal compared to conventional photon therapy. Protons also differ in terms of biological effect compared to photons for the same physical dose. To account for this increased relative biological effectiveness (RBE), a constant RBE of 1.1 is applied in clinical proton therapy treatment planning, i.e. approximately 10% lower physical dose is given to the tumor if proton therapy is used. It is however known that the RBE is not constant, and is dependent on e.g. the linear energy transfer (LET), physical dose and tissue type. By using biological optimization the tumor may get a homogenous biological dose distribution, and prevent over- and under dosage to healthy tissue and the tumor volume. Variable RBE models can be used to optimize a treatment plan with respect to RBE-weighted dose, but these are not yet available in commercial treatment planning systems.

The aim of this study was to implement a method for optimization of treatment plans with respect to both biological and physical dose, and further use this to analyze the differences in physical and biological dose distributions depending on the optimization strategies applied.

Methods: The FLUKA Monte Carlo code was used together with a prototype optimization software to calculate and optimize RBE weighted dose distribution for proton treatment plans. Treatment plan information from the TPS, such as beam energies and positions, was exported and translated to fit the format of the optimizer. The mathematical formulation of three RBE models were also included in the biological dose calculation and optimization; the Rørvik model, the Unkelbach model and the Wedenberg model. These models vary in which parameters they are based on, and therefore provide a good basis for comparison. The different treatment plans consisted of a water phantom with a cubic planning target volume (PTV), three plans for a water phantom with an L-shaped PTV and a small organ at risk (OAR), and a

clinical patient plan. The results from the optimization were verified by running a FLUKA simulation with the original plan, optimizing the result, and then a final FLUKA simulation to verify the dose distribution. The physical dose distributions from the RBE models were compared and a single field optimization of a patient plan was also performed to analyze the dose distribution.

Results: The results from the optimizer showed a homogenous RBE-weighted dose distribution for the different treatment plans and RBE-models. The PTV for all plans received the prescribed dose when the optimized result was verified. Promising results was also achieved from the patient plan where the optimizer provided a relatively even dose distribution although with some discrepancies. The calculations of physical dose distribution from the variable RBE-optimized plans showed in general lower physical dose to the PTV, compared to plans optimized with a constant RBE of 1.1. Physical dose distribution from the plan optimized with respect to the Wedenberg model was also observed to be lower than plans optimized with respect to both the Unkelbach- and Rørvik model. The latter two models showed similar physical dose distributions.

Conclusions: A method for the use of a prototype optimization algorithm was integrated into an existing Monte Carlo based dose calculation framework. The implementation was applied for different RBE models, where the physical dose distributions from the RBE models were compared. Applying variable RBE-models in treatment planning may lead to lower physical dose to the target, thus preventing under- and overdosage to the tumor and surrounding tissue, respectively. Differences between the variable RBE models were also seen, indicating that more research is needed before clinical application.

Contents

Glossary

CT	Computed Tomography
CTV	Clinical Target Volume
DSB	Double Strand Break
DVH	Dose Volume Histogram
GTV	Gross Tumor Volume
GUI	Graphical User Interface
ICRP	International Commission on Radiological Protection
ICRU	International Commission on Radiation Units & Measurements
IMPT	Intensity Modulated Proton Therapy
IMRT	Intensity Modulated RadioTherapy
LET	Linear Energy Transfer
LQ-model	Linear Quadratic Model
MC	Monte Carlo
OAR	Organ At Risk
PB	Pencil Beam
PBS	Pencil Beam Scanning
PHYS	Plan optimized with respect to physical dose
PTV	Planned Target Volume
RBE	Relative Biological Effectiveness
$RBE_{1.1}$	Biological dose calculated with RBE of 1.1
ROI	Region Of Interest
ROR	Rørvik model
SFUD	Single Field Uniform Dose
SOBP	Spread Out Bragg Peak
SSB	Single Strand Break
TPS	Treatment Planning System
UNK	Unkelbach model
WED	Wedenberg model

1. Introduction

1.1 Radiation Therapy

In 2016, over 32,000 people were diagnosed with cancer in Norway, and the number of incidents is growing each year [1]. Typically, more than half of these patients receive radiotherapy during their treatment and the use of radiation treatment is therefore one of the most important modalities in cancer therapy [2]. The goal of radiotherapy is to deliver as much dose to the tumor volume as possible, while at the same time minimizing the dose to the healthy tissue.

The idea of using radiation therapeutically came from E. H. Grubbe in 1896 after suffering X-ray dermatitis because of radiation exposure [3]. He consulted with a doctor about the inflammation on his hand, who saw the beneficial therapeutic application of radiation and urged him to start treating patients with the radiation. Two patients were entrusted to Grubbe and only 60 days after Röntgen had announced his discovery of the X-rays, Grubbe had treated both a neoplastic and an inflammatory lesion in a factory in Chicago.

In recent years, radiotherapy has come a long way from its first applications. One of the big marks in radiotherapy came when computed tomography (CT) was introduced in 1971 by Hounsfield, which gradually shifted the radiation treatment planning from a 2D perspective to 3D [4]. In the 1990s, with multileaf collimators and computer driven algorithms, radiotherapy was revolutionized, and accurate dose distribution to a 3D target became possible. The next leap in radiotherapy came in the early 2000s, with intensity modulated radiotherapy (IMRT). IMRT modulates the intensity of the photon beam during fractionating by using inverse dose planning in a treatment planning system (TPS) [4].

Treatment with highly energetic photons is the most common form of radiation therapy, but has its limitations with respect to dose conformity. Particle therapy, i.e. radiation

therapy with protons and heavier ions, is a treatment method growing around the globe, and consists of using the unique qualities of accelerated charged particles [5]. Protons and heavy charged particles have the ability to deposit their radiation in a more concentrated region compared to photons, and thereby limiting radiation dose to healthy tissue. This is the main motivation for therapeutic use of these particles [6].

1.2 Proton Therapy

In 1946, Robert R. Wilson suggested the use of protons in therapeutic radiation treatment, because of its depth-dose characteristics (Figure 1.1b) [7]. In 1954, only eight years after Wilsons had written about the therapeutic advantages of proton therapy it was applied by researchers at Lawrence Berkley National Laboratory in California to treat a series of patients [8]. Because treatment with protons was novel and highly experimental at the time, the treatments were performed in physics laboratories [9].

In 1990, Loma Linda University Medical Center in California USA became the first hospital with a proton therapy facility, and it was not until ten years later before another hospital-based treatment facility opened [10]. A reason for the modest interest in building proton centers worldwide is the high cost and reward compared to regular photon therapy. It has been calculated that treatment at a proton-only center is 3.2 times more expensive than treatment with photon therapy [11]. Today, 68 proton therapy centers are clinically active worldwide, and many more are under planning, including two centers in Norway [12]. According to the Particle Therapy Co-Operative Group (www.ptcog.ch), close to 175,000 patients worldwide had been treated with particle therapy by the end of 2016 [5].

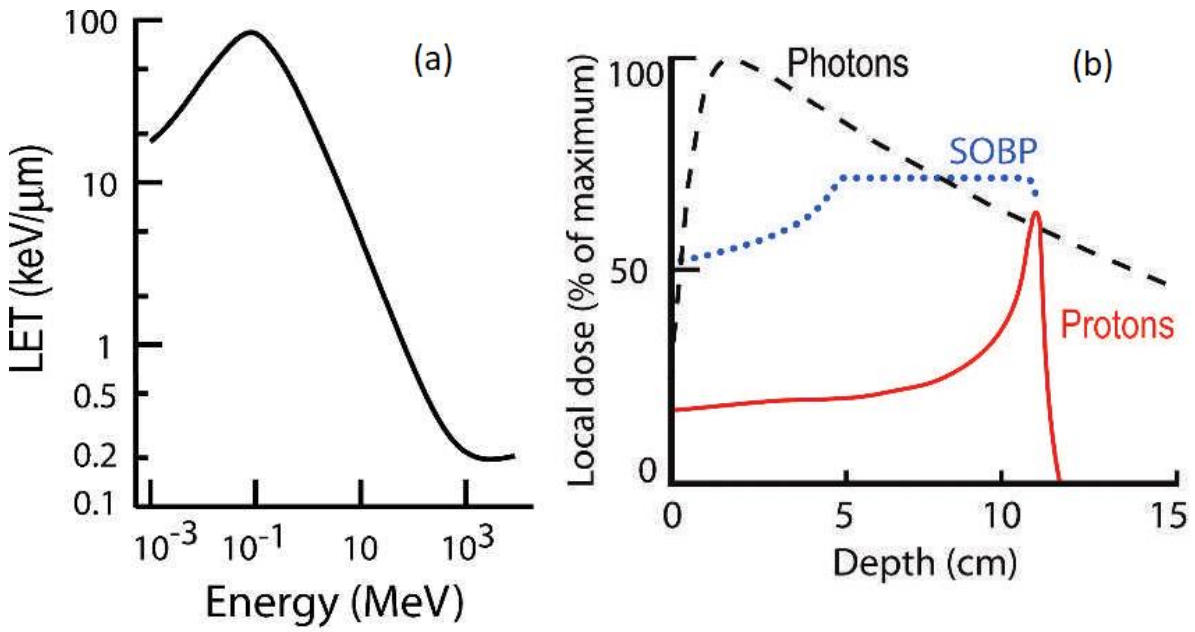

Figure 1.1 (a) Linear energy transfer (LET) of protons vs energy of the proton beam. (b) Depth dose curves for photons (dashed line) and protons (solid line). The dotted lines are representing a spread out Bragg peak (SOBP) for protons [13].

The therapeutic advantage of protons compared to photons is their energy deposition in matter. Protons will slow down as they go through matter, and the energy deposition from the protons will increase with the decreasing velocity. This results in a maximum dose deposition at end of the particle's range, called the Bragg peak (Figure 1.1b). Photons, on the other hand, deposits most of their energy at the beginning of their path, followed by a decrease in dose deposition further into the matter [10].

The linear energy transfer (LET), describes the rate of energy loss per unit length along a particle track, and is typically reported in units of keV/µm. The LET depends on the particle energy (Figure 1.1a) and decreases while the energy of proton increases [13]. Figure 1.1b shows the depth dose curves for photons, protons and a manipulation of multiple proton energies called the spread out Bragg peak (SOBP).

In addition to the different dose deposition between protons and photons, the biological effects, e.g. their ability to kill or inactivate cells, differs due to the different particle-interaction processes. To compensate for this difference, the relative biological

effectiveness (RBE) was introduced, defined as the ratio between the dose of a reference radiation and of protons, when both modalities produced the same biological effect [2]. To account for the increased RBE of protons compared to photons, the physical dose is scaled by a constant and generic RBE-factor of 1.1 in treatment planning for clinical proton therapy [14]. However, experimental data, mainly from *in vitro* cell irradiation experiments have shown that the RBE of protons is not constant and depends on many physical and biological parameters, such as the physical dose, the linear energy transfer (LET) and the photon (α/β)-ratio of the Linear Quadratic (LQ) model [15]. Overall, the experimental data indicates that the assumption of a constant RBE of 1.1 might be too low, especially towards the end of the protons range [14].

1.3 Motivation

The application of a constant RBE of 1.1 ($\mathrm{RBE}_{1.1}$) in clinical proton therapy is a simplification which in principle can lead to both under- and overdosage of the tumor, as well as higher doses to the surrounding healthy tissue than anticipated. The use of variable RBE models in treatment planning and optimization, so-called biological optimization, could therefore increase the quality of treatment plans for proton therapy [16]. For carbon ion therapy, biological optimization is already implemented clinically, however, the RBE effects of carbon ions are larger than the RBE effects of protons [14]. A reason for still using the constant RBE in proton therapy is the uncertainty and complexity introduced by the biological models, and that biological optimization is not currently available in commercial systems for treatment planning. It is therefore of interest to explore how patients can get a more accurate dose distribution when accounting for the variable biological effects, and also quantify the amount of over- and underdosage to the target volume which can occur using $\mathrm{RBE}_{1.1}$. This can be done by optimizing a treatment plan with respect to multiple a variable RBE model and compare to an $\mathrm{RBE}_{1.1}$ optimized treatment plan.

The objective of this study was therefore to implement a system for re-optimization of existing proton treatment plans using variable RBE-models, make it compatible with the in-house tools used for dose verification, and to analyze the differences in physical- and biological dose distributions depending on the optimization strategies applied. The system is based on the FLUKA Monte Carlo (MC) code [17, 18], together with Eclipse treatment planning system (TPS) (Varian Medical Systems, Palo Alto, CA, USA) and a prototype optimization algorithm [19].

2. Physics of particle therapy

High energetic photons and ions are able to ionize the irradiated matter, ejecting electrons from the target atoms [20]. Particle- and photon therapy differ significantly in how the dose is deposited on a micrometer level. These differences have shown to give rise to large differences in biological effect from the same macroscopic dose from photons and protons [9]. This chapter covers the basic interactions of protons with matter, with an emphasis on physical quantities important for modelling of biological effectiveness.

2.1 Proton interactions with matter

Heavy charged particles, i.e. particles with mass greater than the electron, have three main ways of interacting with matter: (a) They are slowed down by Coulomb interaction with the atomic electrons, (b) deflected by Coulomb interaction with nuclei, and (c) undergo nuclear interactions with a nucleus [6, 10]. The interactions are illustrated in Figure 2.1.

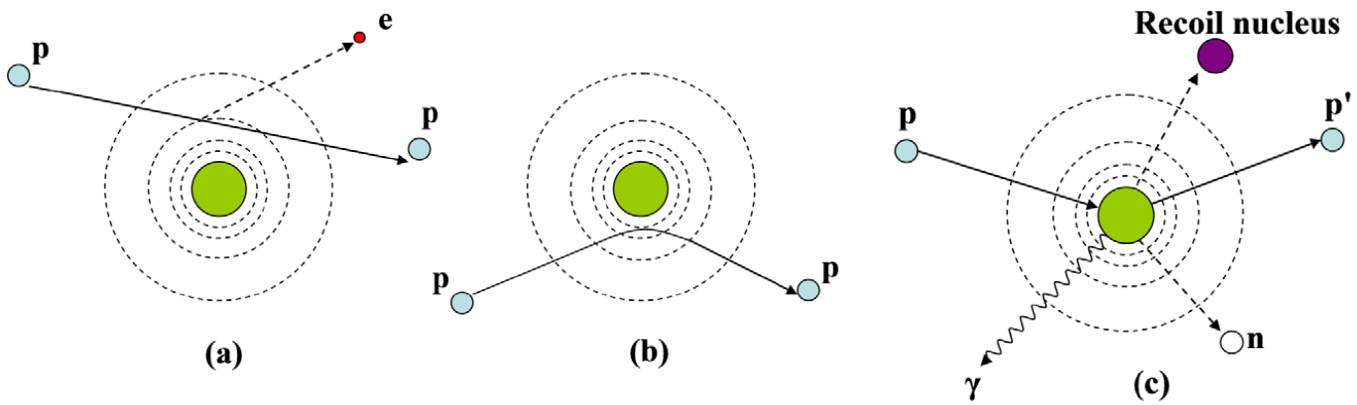

Figure 2.1 Illustration of the three main interactions a proton undergoes: (a) inelastic interactions with the atomic electron, (b) Coulomb-scattering and (c) nuclear interactions [21].

2.1.1 Inelastic interactions with the atomic electron

The primary source of energy loss is the Coulomb interaction with the atomic electrons (Figure 2.1a). A proton will lose a small fraction of its energy to an atomic electron either by excitation of the electron to a higher shell or by ionization of the electron, which removes it completely [22]. Since the mass of a proton is far greater than the mass of an electron, the proton will not deviate much from its original trajectory after the interaction. The majority of secondary electrons made from this interaction will only travel a short distance from the proton-path while ionizing and depositing energy. These electrons are called delta rays [10].

The complex interaction between the charged particle and atomic electrons represents the electronic stopping power and is described by the Bethe-Bloch formula [23, 24]:

$$-\frac{dE}{dx} = 2\pi N_a r_e^2 m_e c^2 \rho \frac{Z}{A}\frac{z^2}{\beta}\left[\ln\left(\frac{2m_e\gamma v^2 W_{max}}{I^2}\right) - 2\beta^2 - \delta - 2\frac{C}{Z}\right] \quad (2.1)$$

where dE is the energy loss over a track segment dx. The remaining parameters are described in Table 2.1.

Table 2.1 Description of the variables in the Bethe Bloch equation

Variable	Description	Variable	Description
N_a	Avogadro's number	I	Mean excitation potential
M_e	Atomic mass	ρ	Density of the absorbing material
Z	Atomic number of the material	W_{max}	Maximum energy transfer from a single collision
A	Atomic mass of material	γ	Lorentz-factor
z	Charge of the incident particle	δ	Density correction
$\beta = v/c$	Relativistic velocity	C	Shell correction
v	Speed of incident particle	c	Speed of light in vacuum
r_e	Classical electron radius		

The Bethe-Block formula describes how much energy, dE, a charged particle loses along a track segment dx, in matter. The last two terms of the Bethe-Block equation is correction terms which includes quantum mechanics and relativistic effects, and requires very high or very low energies to be considered [21]. An important aspect of the Bethe-Block is how the projectiles characteristics affect the energy loss. It can be seen that the energy loss is proportional to the inverse square of the velocity, and the square of the ion-charge. It is not dependent on the mass of the projectile, but relies heavily on the absorber's mass density [21].

2.1.2 Coulomb scattering

If the proton passes close to the nucleus, it will be deflected by the Coulomb repulsion of the positive charged nucleus. This is referred to as Coulomb scattering (Figure 2.1b). Although the deflection of each interaction might be small, the sum of all the deflections can lead to a high lateral spreading of protons [10]. It therefore is necessary to take into account the Coulomb scattering in dose calculations of dose distributions in phantoms or patients with treatment planning systems [21].

2.1.3 Nuclear interactions

If the distance of approach between the nucleus and proton becomes too small, the proton may undergo nuclear interactions with the nuclei in form of scattering (Figure 2.1c). Although the probability of scattering is small, it will increase with the number of nuclei in the target and with the energy of the proton. It is estimated that around 20% of protons with high energies undergo nuclear interactions [10]. Nuclear interactions can be defined as elastic or non-elastic. In an elastic nuclear interaction, the nucleus will only recoil and the total kinetic energy will be conserved. However, in non-elastic collisions, the target nucleus will absorb some of the kinetic energy and might undergo several nuclear interactions, such as disintegration, emission of prompt gamma rays etc. The recoil nucleus will be absorbed at the point of interactions, while the secondary

particles, protons and neutrons, will travel a relatively large distance and produce a halo of low dose around the beam [10].

2.1.4 Range straggling

An important aspect of the stopping power is that it is only an average value for the energy loss per unit distance, and real life fluctuation will occur. This is known as energy-loss straggling, or range straggling [25]. A theory by Janni [26] postulates the standard deviation of range straggling as a percentage of the mean projected range. For light materials the range straggling for protons is about 1.2 %, and slightly higher for heavy materials [6].

2.1.5 Absorbed dose

The absorbed dose D is the basic physical dose quantity and is used for all types of radiation and every type of geometry. The definition is quotient of energy $d\bar{\varepsilon}$ imparted from ionizing radiation to a matter of mass dm. The dose is therefore given as

$$D = \frac{d\bar{\varepsilon}}{dm} \tag{2.2}$$

The SI unit for absorbed dose is Gray (Gy), or J/kg [27]. The absorbed dose is insufficient when it comes to predicting probability of health effects resulting from unspecified conditions. The International Commission on Radiological Protection (ICRP) suggested weighting factors to account for the delayed stochastic effects [28].

In proton therapy, the terms physical dose and biological dose are used, where the physical dose equals the absorbed dose.

2.1.6 Spread-out Bragg Peak

The Bragg Peak (Figure 1.1b), is made up by the sum of the three proton interactions, and is where the proton deposits maximum energy [13]. The depth of the Bragg peak is energy dependent, and by using a large set of beam energies, the whole tumor-

volume can be covered by a uniform dose along the beam axis. The plateau of the different energies is called the spread-out Bragg peak (SOBP) [29] (Figure 2.2).

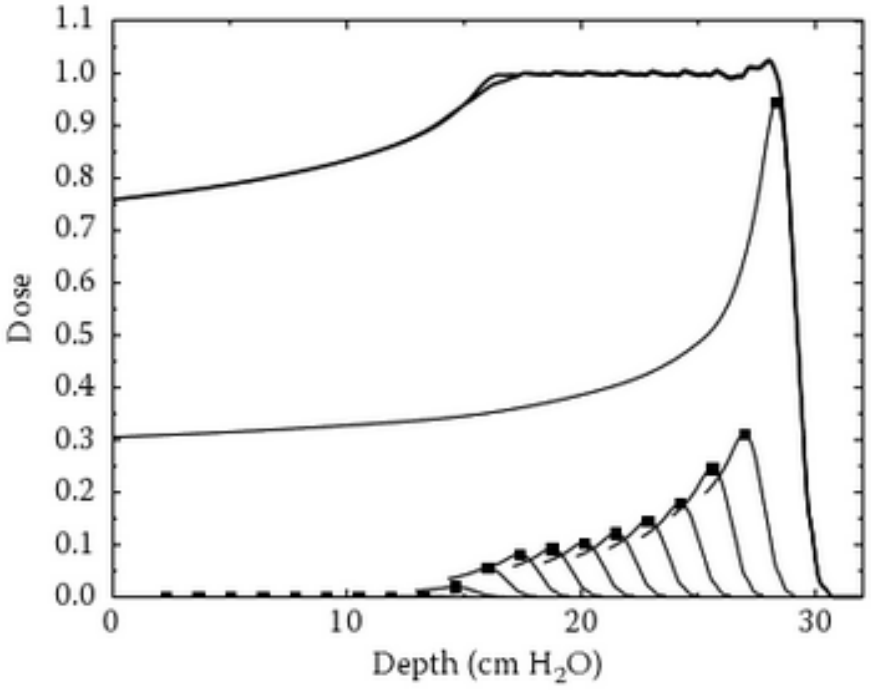

Figure 2.2: Manipulating several individual Bragg peaks to make a flat dose distribution. This is called a Spread-Out Bragg peak (SOBP) [6].

2.2 Linear energy transfer

There is a difference between the amount of energy deposited in the medium by a charged particle and how the energy is absorbed by the medium [30]. To describe this difference, Zirkle [31] introduced the linear energy transfer (LET), and defined it as the energy, dE, transferred from fast charged particles per unit length, dx, of their paths, to the biological material in on near these paths [31]. The LET is normally given in the unit $\mathrm{keV}/\mu\mathrm{m}$, and can mathematically be written as:

$$LET \equiv \frac{dE}{dx} \tag{2.3}$$

The LET of protons will increase inversely with the proton velocity. Because of this energy deposition, protons will lose energy at an increased rate further into a uniform medium, and therefore deposit more and more energy until they stop. The LET is therefore a measure of the rate of energy loss per unit length along a particle track and reflects the number of ionizations created along the track [13]. For protons, the LET is relatively low until the end of their range. Then, when the protons approach the end of their range, the LET rises drastically. This gives protons as well as other heavy charged particles, an advantage in that they deposits most of their energy at the end of their path. This property utilized in proton therapy treatment [13].

Most of the particle energy is lost due to the inelastic interaction with the atomic electrons, as described by the Bethe-Block formula (equation (2.1) although a small portion of the energy is converted to bremsstrahlung or long distance delta rays [30]. The LET with a cutoff energy to restrict the energy from delta rays is called the restricted LET, denoted LET_{Δ}. If no cutoff from the delta rays is considered, the LET is equal to the electronic stopping power S_{el}, written as

$$LET \cong S_{el} \tag{2.4}$$

From the original definition of LET, two different practical concepts are derived. The track-averaged LET (LET_t) and the dose-averaged LET (LET_d). When biological outcome is the focus of a study, the LET_d is generally the value used because it considers both LET and dose [32]. LET_d can be calculated as follows:

$$LET_d(z) = \frac{\int_0^\infty S_{el}(E)D(E,z)dE}{\int_0^\infty D(E,z)dE} \tag{2.5}$$

where $S_{el}(E)$ is the electronic stopping power of a primary charged particle with kinetic energy E and $D(E,z)$ is the absorbed dose contributed by a primary charged particle with kinetic energy E at a location z [32].

3. Radiobiology

3.1 Biological damage by radiation

An important aspect of radiotherapy is to understand the damage radiation does to biological tissue. When radiation interacts with tissue, its energy will be converted and deposited in the tissue [33]. Observed radiation effects can broadly be classified into two groups, stochastic and non-stochastic effects. Stochastic effects occur randomly and the probability of incidents is decided by the dose. An example is cancer, which can occur without known exposure to radiation [34]. Most biological effects fall under non-stochastic effects, or deterministic effects. There are three qualities that categorizes the deterministic effect: A minimum dose must be exceeded for observable effect of the radiation, the magnitude of the effect grows with the dose, and there is a casual relationship between the radiation and the observable effects [34]. A comparison between the two effects is given Figure 3.1.

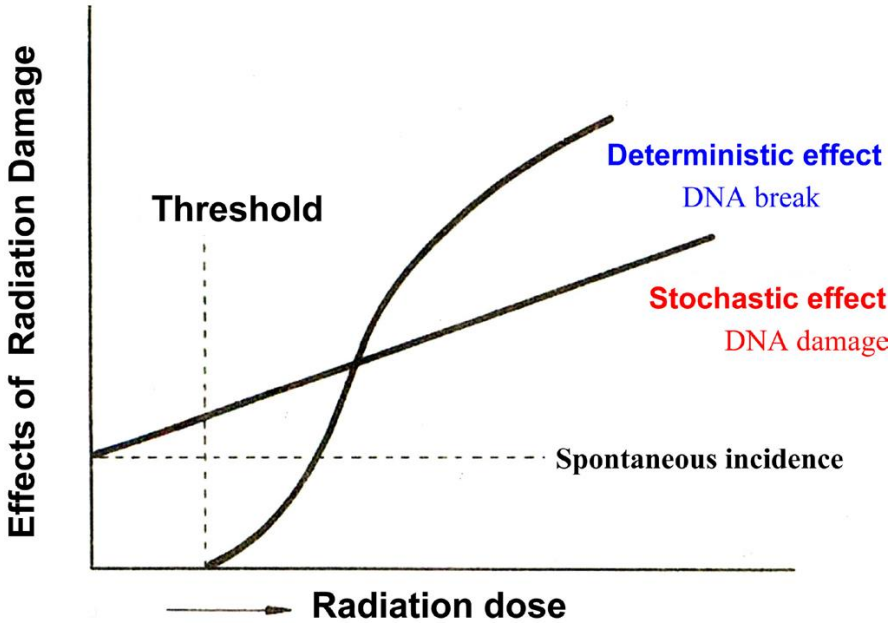

Figure 3.1 Classification of radiation effects [2].

When a cell is exposed to radiation, the most vulnerable material is the DNA [35]. Cell death induced by radiation is therefore mainly attributed to radiation damage of the DNA. Radiation can damage the DNA in two ways, either by direct action or by indirect action. With direct action, the radiation hits the DNA directly and disrupts the molecular structure. This is the lead process for radiation with high LET, such as α-particles and neutrons, high energy doses, and low energy (i.e. high LET) heavy charged particles in general [36]. When radiation ionizes the water, it leads to chemical reactions that threaten the DNA with highly reactive radicals. This is indirect radiation effect on the DNA. For low LET radiation, the most common radiation effect is through the delta-rays creating free radicals, while direct action is more relevant for higher LET radiation [6].

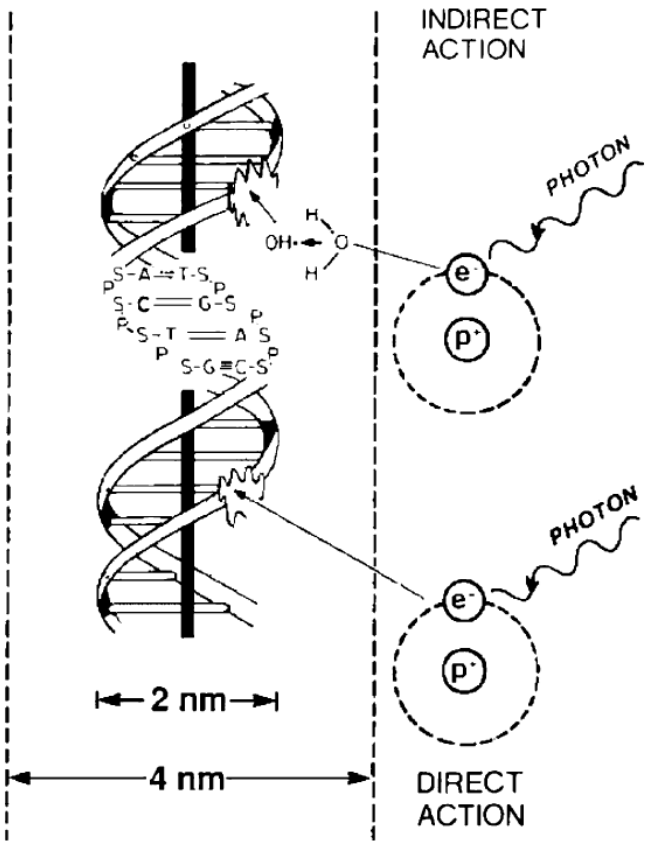

Figure 3.2 Direct and indirect action of radiation [1]

The most common damages to the DNA from radiation are base damage, single strand break (SSB), and double strand breaks (DSB). The DSB is often considered the critical

lesion and is believed to be the main cause of late and early effects from ionizing radiation. An even more complex damage occurs when there are two or more types of lesions nearby in the same DNA. These clustered lesions are very difficult to repair, and is postulated to be responsible for lethal and mutagenic effects of ionizing radiation [13].

When the DNA is damaged, it will try to repair itself and failure to repair itself gives rise to mutations and chromosomal abnormalities. An important strategy to avoid and guard against the mutations is cell death [37]. The most commonly applied model which describe the radiobiological effects and cell death is called the linear quadratic model (LQ-model). It describes the surviving fraction S of cells after they are irradiated with a dose D, and is given by:

$$S(D) = e^{-\alpha D - \beta D^2} \tag{3.1}$$

Here α and β are tissue specific parameters. The parameters can be correlated to respectively single track events and double track events; at low doses the α will dominate, while at higher doses, more strands on the DNA will break and the β will dominate [2, 38].

3.2 Relative biological effectiveness - RBE

The relative biological effectiveness (RBE) of protons is the ratio of the dose of a reference radiation, gamma or MeV X-rays, to protons, needed to produce the same biological effect [2]. The effect can be quantified by measuring a biological endpoint of irradiated cells or tissue, like the median lethal dose or a specific clonogenic survival level, i.e. a certain fraction of cells surviving an irradiation [13]. The RBE is mathematically defined as:

$$RBE(endpoint) = \frac{dose\ of\ reference\ radiation}{dose\ of\ test\ radiation} \tag{3.2}$$

when the dose of the reference radiation and of the test radiation results in the same biological effect.

For proton therapy, clinical treatment planning is performed with an RBE of 1.1. However, it is widely agreed upon that the RBE is not constant, and in many instances higher than 1.1, especially in the distal part where the LET is high [14]. To account for the difference in RBE between particles and photons, treatment plans in particle therapy can be optimized applying the RBE-weighted dose (R_{RBE}), also called biological dose:

$$D_{RBE} = RBE \times D \tag{3.3}$$

where, D is the physical dose. In particle therapy, the biological dose is given in Gy(RBE), replacing the previous used dose-equivalent and cobalt-Gray equivalent.

In spite of many years of research, the RBE is still the main source of uncertainties when it comes to dose estimation in charged particle therapy [14]. As mentioned, a constant RBE of 1.1 is used clinically in proton therapy, but it is acknowledged that the variation in RBE ideally should be corrected for, especially around the distal part of the SOBP and in the distal dose falloff. This increase of RBE also causes a shift in the biological effective range and enhances the effective beam range and from Figure 3.3 it can be seen that the shift in range can be up to several millimeters [14]. A reason for why this generic RBE-value is still in use is due to the lack of biological input parameters. This leads to lack of RBE-values in all tissues in the treatment planning process, and therefore the generic RBE is still recommended for clinical use [39].

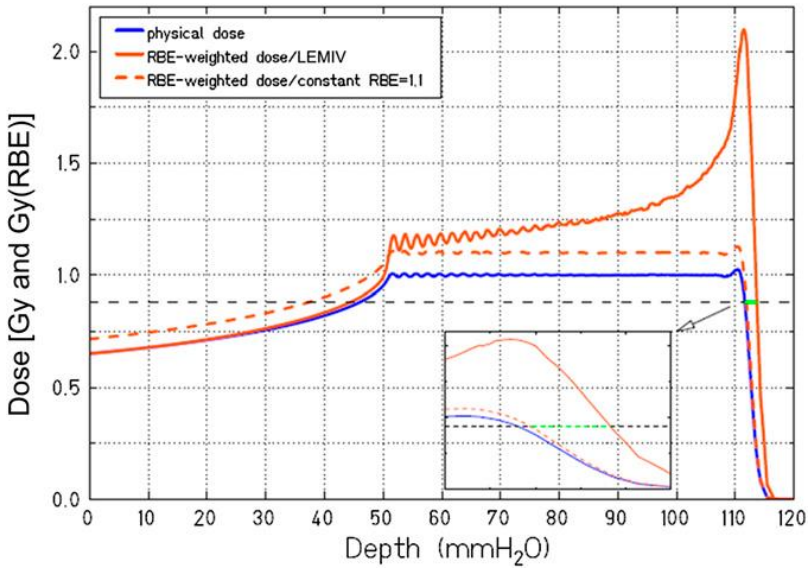

Figure 3.3 Biological range extension for proton, where the blue line is the physical dose, the dashed orange line is the biological dose with constant RBE of 1.1 and solid orange line is the biological dose calculated using a variable RBE model (the LEMIV) [14].

In vitro studies of the RBE show a bell shaped dependency of the LET-value (Figure 3.4), and also a dependence on the particle charge [14]. It is also been shown that the RBE dependence on several other different factors, which often are independent of each other. These factors are for example dose, biological endpoint, tissue type, dose, and proliferation i.e. the rate of repopulation [14].

As mentioned above, the RBE of proton increases towards the end of the range, which has been reported by *in vitro* cell survival experiments. From the experiments, depending on different parameters, it can be seen that RBE increase from around 1.0 and 1.1 in the entrance region, to about 1.3 in the Bragg-peak and 1.6 in the falloff region [40]. However, the absolute values of RBE has been shown to be strongly dependent (inversely proportional) on dose [40], and estimates of RBE also varies significantly between different RBE models. The explanation for this rise in RBE is that the LET increases towards the end of the particle range. The correlation can be seen in Figure 3.4.

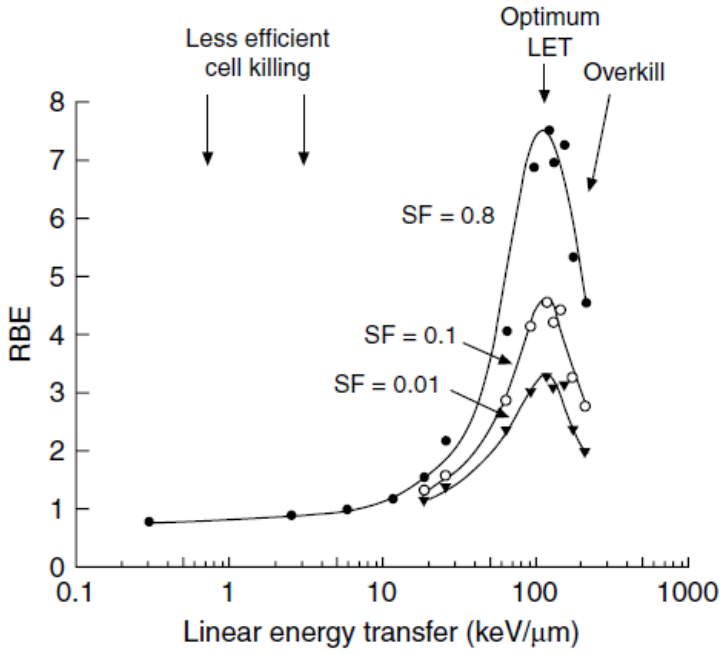

Figure 3.4 Relationship between RBE for cell killing and LET [2]. The RBE has been calculated at surviving fraction (SF) levels of 0.8, 0.1 and 0.01 for helium-ions.

3.2.1 Biophysical models for the prediction of the RBE

There are several different models for calculating RBE, and most of them are based on the LQ-model. The derivation of a generic expression of the RBE from the LQ-model is described in the following. From the LQ-model (equation (3.1)), the photon and proton dose at the same survival level is described as follows:

$$S = e^{-\alpha D - \beta D^2} = e^{-\alpha_x D_x - \beta_x D_x^2} = S_x \tag{3.4}$$

where D is the dose, and all quantities with subscript x represents photon radiation, while the others represents proton radiation. Solving this secondary equation for the positive roots of D_x gives:

$$D_x = -\frac{1}{2}\left(\frac{\alpha}{\beta}\right)_x + \sqrt{\frac{1}{4}\left(\frac{\alpha}{\beta}\right)_x^2 + \frac{\alpha}{\alpha_x}\left(\frac{\alpha}{\beta}\right)_x D + \frac{\beta}{\beta_x}D^2} \tag{3.5}$$

From this, together with the definition of the RBE, a generalized expression for the RBE can be given as

$$RBE(D, \alpha, \alpha_x, \beta, \beta_x) = \frac{D_x}{D} = \frac{1}{2D}\left(\sqrt{\left(\frac{\alpha_x}{\beta_x}\right)^2 + 4D\frac{\alpha_x}{\beta_x}\frac{\alpha}{\alpha_x} + 4D^2\frac{\beta}{\beta_x}} - \frac{\alpha_x}{\beta_x}\right) \tag{3.6}$$

Here, D/D_x is the physical dose and, α/α_x and β/β_x is biological tissue-parameters of the LQ-model, for protons and photons, respectively [15, 41]. Further, by evaluating the upper and lower physical dose limits, an expression for the extreme RBE at low and high doses can be found [42, 43]:

$$\lim_{D\to 0} RBE = RBE_{max} = \frac{\alpha}{\alpha_x}. \tag{3.7}$$

$$\lim_{D\to \infty} RBE = RBE_{min} = \sqrt{\beta/\beta_x}. \tag{3.8}$$

Equation (3.6) can therefore also be written as

$$RBE\left(D, \left(\frac{\alpha}{\beta}\right)_x, RBE_{max}, RBE_{min}\right) = \frac{1}{2D}\left(\sqrt{\left(\frac{\alpha}{\beta}\right)_x^2 + 4D\left(\frac{\alpha}{\beta}\right)_x RBE_{max} + 4D^2 RBE_{min}} - \left(\frac{\alpha}{\beta}\right)_x\right) \tag{3.9}$$

While all LQ-based RBE models have equation (3.9) in common, they differ in the definition of RBE_{min} and RBE_{max} [44]. The RBE models which have been applied in this project are described in chapter 5.4.

4. Treatment planning

The aim of treatment planning is to optimize the dose distribution to a target volume, and minimize the dose for the surrounding normal tissues. The planning is done by a simulation software also known as a treatment planning system (TPS), which estimates the treatment delivery system to deliver a uniform dose to the target volume [45].

With radiotherapy as any other medical procedure, there is a balance between risk and benefit [2]. Treatment planning is therefore an act between maximizing the probability of curing the patient (Tumor Control Probability), and minimizing the probability of serious side effects (Normal Tissue Complication Probability) [6].

4.1.1 Uncertainties

There are always uncertainties when it comes to dose and dose distribution. An aim, suggested by international regulatory bodies, is that the delivered dose should be within 2.5% of the prescribed dose [9]. Dose calculations are done routinely using analytical algorithms in traditional photon therapy, but have shortcomings in proton therapy. Monte Carlo (MC) simulations is considered the gold standard in dose calculations, and although previously deemed too slow for clinical use, recently achieved the efficiency that can make them suitable for clinical treatment planning [9].

4.2 The treatment planning process

The process of planning and improving cancer treatment relies on modelling. A model which accurately describes the transport of the beam through the patient is needed, as well as a model that describes the biological consequences of the beam. This includes RBE-models which converts different biological parameters into RBE-weighted dose [46].

The first step of treatment planning is to acquire images (normally computed tomography (CT)) of the patient to review the extent of the tumor, and also localize organs at risk (OAR) [45].

The second step in the treatment planning process is segmentation. From the images, medical doctors and physicist define the volumes of the patient, such as the target volume and the OARs [45]. The most important volume is the planned target volume (PTV), to which the prescribed dose should be delivered. The PTV is a delineation of the tumor volume, with safety margins according to the International Commission on Radiation Units (ICRU). The medical doctor will first define where the visible tumor is in a Gross Tumor Volume (GTV), and then expanding it into a Clinical Target Volume (CTV), to account for the invisible spread of cancer cells. The last step in the delineation is to account for the uncertainties in the dose delivery and target movement into the PTV [6]. Any OARs are also delineated and prescribed a maximum dose in this process [45].

4.3 Treatment planning techniques

In clinical particle therapy, there are two main techniques to deliver homogenous dose to a target, passive scattering and active scanning, the latter also termed pencil beam scanning (PBS). There are advantages and disadvantages for both techniques, but scanning has properties which makes it the better option when it comes to optimize dose to a target, and is the technique implemented in all new proton therapy centers. PBS is a technique that moves a beam of charged particles over a target volume and can be seen in Figure 4.1. Different properties can be modulated during the scanning, as position, size, energy (and thus range) and intensity of the beam. A specific beam setup is known as a spot. Magnets are used to manipulate the beam position across the treatment field [6].

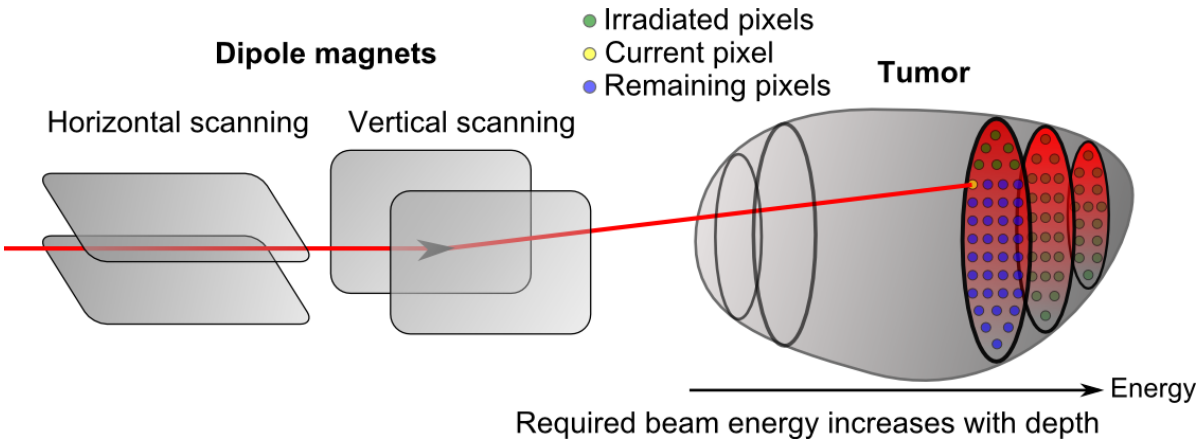

Figure 4.1 The technique of pencil beam scanning [47]. The dipole magnets manipulate the beam to the shape of the tumor.

Intensity modulated proton therapy (IMPT) is a treatment technique which delivers a non-uniform dose distribution in each treatment field. The process begins with the desired dose distribution, and using algorithms to arrive with specification of the required dose fluence. This way of planning is called inverse planning [48]. Intensity-modulation methods achieve the highest conformity of proton dose distribution to the target volume and spare most of the healthy tissue. The beam will change energy and intensity to control the dose to a point. The most common technique when it comes to IMPT is the 3D modulation method, where different Bragg peak spots are placed in the volume and are all individual weighted [6].

4.4 Monte-Carlo simulations

MC simulations take into account the physics and interaction of particle-by-particle by using theoretical models or experimental cross section data. Tissue inhomogeneity is also considered in the MC simulation, by using parameters like material properties, atomic elemental composition, electron density, and mass density. One of the main advantages of these codes is that they can be used for as for dose validation purposes. Another advantage is that it can simulate the different components on the treatment head and extract parameterized phase spaces for complex beam delivery systems. Although the main MC codes (FLUKA, GEANT4 and MCNPX) were initially

designed for particle and nuclear physics use, they have been successfully integrated into the field of particle therapy [45].

How accurate the output from a MC-simulation is, depend on the number of particles. The uncertainty for a simulation with *N* events is therefore proportional to $1/\sqrt{N}$ [6].

4.5 Optimization problem

For optimization methods, limitations and treatment goals need to be defined mathematically, respectively called constraints and objectives. The image data from the patient is therefore partitioned into volumes called voxels, which then includes the necessary data, as OAR and other tissue volumes. These voxels are further made into geometric objects called region of interest (ROI).

The total dose from an IMPT field is the sum of all distributions from the static pencil beams at various positions along the particle track. The dose to voxel i from pencil beam j , can be written as

$$d_i = \sum_j x_j \cdot D_{ij} \tag{4.1}$$

where x is the relative weight of beam j. The weighting variable needs to be determined in the treatment planning. Since thousands to tens of thousands pencil beams are used, mathematical optimization methods are used in IMPT. The output of the optimization is called the fluency map, and is a set of the beam weight distributions.

An objective for voxels or volumes can be defined in the plan, and these are expressed in objective functions. An objective function which is widely used is the quadratic penalty function. This typically aims at minimizing the volume, within the OAR, that exceeds the maximum tolerance dose D^{max}. It is given by:

$$O_n(d) = \sum_{i \in OAR_n} H(d_i - D^{max})(d_i - D^{max})^2 \tag{4.2}$$

where H is the Heavyside function which is zero for negative values and one for positive values. Similarly, there are quadratic functions that minimize tumor volumes that which receives less than a minimum dose D^{min}. Another constraint may be that every voxel in the ROI should be between a minimum dose and a maximum dose, which would lead to the hard constraint of:

$$D^{min} \leq d_i \leq D^{max} \quad \forall i \in VOI \tag{4.3}$$

A problem with constraints and objectives is that they are often in direct conflict with each other in clinical situations. The solution to this problem is often to rewrite the constraint as an objective and change the different weightings for the objectives. An example of a conflict is when a target is not completely radiated because a critical structure lies next to it. The solution is to minimize the dose to the OAR that exceeds the dose limit instead of enforcing the dose around to be below the maximum limit. Such an objective is called a soft constraint [6].

4.6 Biological optimization

Optimizing a treatment plan with respect to biological dose with variable RBE models is a growing topic in proton therapy. The limited ability to predict RBE distributions is one of the reasons why a constant RBE of 1.1 is used in clinical practice [49]. When RBE calculations are integrated into the optimization process, computational requirements becomes an issue, because the RBE is calculated for each iteration [16].

The non-constant RBE value causes a dilemma when it comes to treatment planning, especially for IMPT. A higher RBE value than expected will lead to higher dose and more normal tissue complications. LET-hotspots may also occur in critical structures due to the physics and dose planning. Because of these uncertainties, RBE-based IMPT-planning is not used in clinical therapy yet [50].

The first step in biological optimization is defining an RBE-model for the RBE and biological dose. In this thesis, we have focused on three models described in detail in chapter 5.4. These models are dependent on the LET and tissue specific parameters within a target volume or OARs. As LET varies spatially within the patient, LET calculations are needed for the RBE-models. With all the parameters, a new objective function can be made, similar to the one described in section 4.5, only with respect to RBE-weighted dose, rather than physical dose. This can be done by two objectives; homogenous biological dose in the volume or homogenous LET distribution in the volume [16].

5. Materials and Methods

This chapter will describe the process of re-optimizing an existing treatment plan with respect to different biological models. An overview of the process is given in Figure 5.1 with the descriptions found in Appendix A In short, the information about the treatment plan, optimized with $RBE_{1.1}$ from the Eclipse treatment planning system, were modified into a format usable as input in the FLUKA MC code. Then, MC simulations were run, and the output from the MC-simulation was directly used in a prototype optimizer. The optimizer modifies the weighting of the individual pencil beams (PBs) in the existing plan, with respect to a biological model chosen by the user. A second FLUKA-simulation with the now biological optimized plan was performed to generate the final dose distributions.

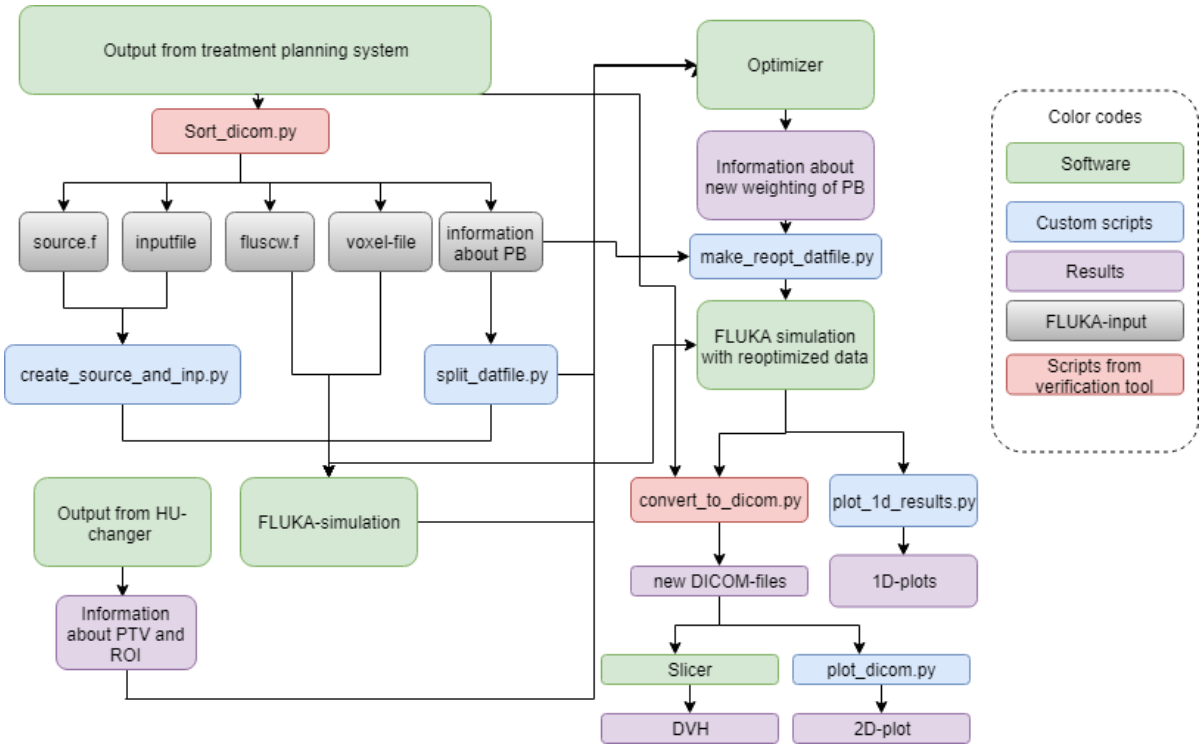

Figure 5.1 Flowchart of the re-optimization process. Explanation of the different files can be found in Appendix A

5.1 Software

5.1.1 Eclipse treatment planning system

The Varian Eclipse treatment planning system is used at the Haukeland University Hospital. It can create treatment plans for many different radiation treatment modalities, including proton therapy. The exported treatment plans are given in DICOM (Digital Imaging and Communications in Medicine)-format. DICOM is the standard format for storing information in medical imaging.

5.1.2 Optimizer

A prototype optimizer [19] was used to optimize the treatment plans. The optimization program used information about the pencil beams, information about the physical dose, the biological variables α and β from FLUKA, and a file with information about which voxels in the CT image to irradiate (i.e. to irradiate the PTV while avoiding OARs). The cell-line for the chosen biological model has to be manually imported into the program. The program will use all the above information to calculate the best weighting scheme for the plan, with respect to the biological model.

The optimizer (written in C++) is currently only run by employing a shell script, i.e. not with a graphical user interface (GUI). The shell script offers multiple options for the optimization process such as cell-lines, options for constant RBE and conversion criteria. In this project, the result was deemed sufficient when the cost function was below 1% i.e. the percent change between each iteration was lower than 1.

The optimizer is made for the FLUKA implementation of the Centro Nazionale di Adroterapia Oncologica (CNAO) beam line. Here, beams are sent into the patient from different angles by rotating the patient, while the beam always comes from the same direction (z-direction). This is not similar to Eclipse, which makes plans where the gantry is rotated. The script sort_dicom.py was therefore modified to provide beams

from z-direction. The files received from CNAO was made for carbon-ion therapy plans, but has been changed to fit proton therapy plans.

5.1.3 FLUKA

The FLUKA MC code [17, 18] was used together with its interface, FLUKA advanced interface (FLAIR) [51]. The FLUKA development version was used in this project, as the optimizer required output from this version of FLUKA.

FLUKA can be used with several subscripts, where the ones used in this project were the source and fluscw routine. The source routine reads in information about the pencil beam and converts the information so it can be read by FLUKA. The fluscw routine (which in essence is a fluence weighter) enables scoring of the biological parameters by choice, as dose is given by $fluence \times LET\ /\rho$, where ρ is the density of the material. Treatment planning systems calculate dose to water, and to enable direct comparisons we did the same, making the density of water, i.e. $1\mathrm{g/cm^3}$. A table containing α and β values is included in the fluscw routine, and multiplied with $fluence \times LET$, to achieve the biological variables needed for biological dose. In FLAIR, the Hounsfield units in the CT image can be converted into material density and element composition [52, 53]. This results in the VOXEL-files used in the simulation.

The statistical uncertainty is calculated by FLUKA, and is dependent of number of primaries used in each simulation. Since statistical errors of MC simulations is dependent on $1/\sqrt{N}$, where higher statistics would lead to lower uncertainties. In this work, the number of primary histories needed to achieve reasonable low uncertainties were evaluated in each separate scenario as this varies with the beam properties and the geometry used in the simulation. Typical number of primary histories ranged from 4000 to 20000 per primary.

5.1.4 3D Slicer

3D Slicer [54] is an open software for medical imaging and informatics. Slicer reads DICOM-files and allows the user to create 2D-plots, and dose volume histograms (DVHs). The extension SlicerRT is needed for DVH calculations [55]. In this project, Slicer was mainly used to achieve data for DVHs.

5.2 The optimization process

5.2.1 Intital simulation before the optimization

The first step is to convert the DICOM-files into a format which is readable for the FLUKA MC program. This was done by using modified scripts originally created by Lars Fredrik Fjæra [56]. The output from the conversion includes a FLUKA input file and a file with the preliminary information about the pencil beam. The output also includes the standard subroutine scripts needed for the FLUKA MC simulation, i.e. the source and fluscw routines. The modification made for this project consisted of changing the direction of the beam, so it always came from the same direction.

The aforementioned FLUKA-files had to be modified to fulfill the requirements of the optimization program. The file containing information about the pencil beams was split into multiple files, one for each core, using a python script created for this master project. Previous simulations in the group had been done by rotating the beam and leaving the patient in the same position, however, the optimizer requires the beams to always come from the same direction, and instead rotate the patient. This lead to a modification of the scoring cards so that the patient and the region of interest (ROI) were rotated instead the beam. In order to obtain sufficient statistics during the simulation process, the optimizer requires the total number of simulated primaries to be 5000 times larger than the number of pencil beams i.e. 5000 primaries per spot. The exported output from the FLUKA simulations were the physical dose, D, as well as αD and $\sqrt{\beta}$.

5.2.2 The optimization process

The next step is to use the optimizer to achieve an optimized plan with respect to the different biological models. The optimizer reads in physical dose, αD and $\sqrt{\beta} D$ event by event values from the initial FLUKA simulation, as well as information about the pencil beams and information about the location of the PTV and OARs. The different ROIs are achieved using the Python script HUchanger.py, which reads in the DICOM-files, and defines the voxels that belongs in the PTV and OARs.

The output from the optimizer includes information about the new pencil beam weights, and different plots for every 10^{th} iteration. These plots include dose volume histograms (described in chapter 5.2.3), and dose distributions. Examples of these plots can be found for each treatment plan in Appendix D .

5.2.3 Plan verification and plotting of the results

Before running the FLUKA-simulation for dose-verification, the information about the new weighting achieved from the optimizer must be converted into a format readable by FLUKA. A Python-script was created for this purpose, which replaces the original weights with the newly optimized weights in the original treatment plan. For the FLUKA-simulation, the scripts and method from the original dose verification tool are used, except for the modified file with the pencil beam information, and a modified scoring card. The output from the FLUKA-simulation is converted back into DICOM-format and plotted by using modified scripts originally made by Fjæra [56]. For the dose volume histograms (DVHs), the open source software 3D Slicer is used, while Python scripts are used for the 1D plots.

A DVH evaluates the dose distribution in a volume of interest and can be defined as the summed volume of elements receiving dose in a specified dose interval, against a set of equally spaced dose intervals [25]. The most frequently used is the cumulative

DVH which display the amount of volume receiving a dose greater than, or equal to the given dose, plotted as a function of dose. Cumulative DVHs will be displayed in this project.

For the cubic PTV in the water phantom, the different RBE-weighted doses were also compared to each other, when the plan was optimized with respect to physical dose (RBE = 1.0).

5.3 Applied treatment plans

The optimization process was first tested on a simple cubic PTV in water, before proceeding to a more complex L-shaped PTV shape in water. The L-shaped volume was chosen to detect potential errors in the beam and patient rotation. Finally, the optimizer was tested on a patient plan.

5.3.1 Cubic PTV in water

The plan for the water phantom was made in the Eclipse TPS for Johan Martin Søbstad's master thesis [57]. The phantom is $30 \times 30 \times 30$ cm^3, and the region of interest is a PTV with a volume of $4 \times 4 \times 4$ cm^3 placed in the center. The phantom was initially prescribed a total dose of 2 Gy($RBE_{1.1}$). An illustration can be seen in Figure 5.2.

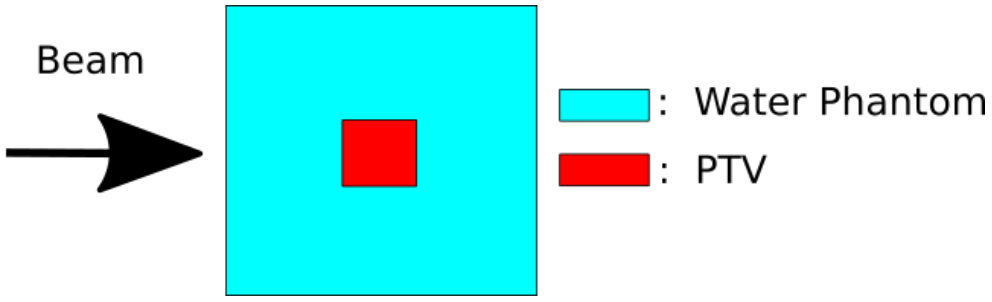

Figure 5.2 Illustration of water phantom (turquoise), PTV (red), and beam direction.

Another water phantom plan was also made in the TPS, without using DICOM image files. Further description, as well as results, of this plan can be found in Appendix B

5.3.2 L-shaped PTV in water

While the cube in water could reasonable indicate if the optimization process was working or not, it is a symmetric volume and would therefore not provide us with information about potential problems with rotations of the coordinate systems. As we have many files which have to be rotated correctly, it would be useful to also test the optimizer on a shape which is asymmetric. New plans were therefore made for a water phantom with a PTV shaped like an L, hereby denoted L-PTV. The plan also included a small OAR placed next to the L-PTV. The L-PTV was defined for this master project in the Eclipse TPS alongside three separate plans. Each of these three separate treatment plans had different fields, and will be described below.

The first plan (Plan 1) consists of one field, coming in the lateral direction of the L-phantom (Figure 5.3). This field is common for all three L-phantom plans.

The second plan (Plan 2) consists of two perpendicular fields, where the first enters in lateral direction, while the second field enters in inferior direction, which is perpendicular to the first field.

The third plan (Plan 3) also consists of two fields, where the first field enters in the lateral direction of the L-phantom, while the second field enters from a gantry angle of 293° and treatment table rotation of 60°. This field is denoted angular field. The reason for the second angle is to map how the PTV, OAR, voxels, and fields are rotated in the optimization process. Figure 5.3a shows an illustration of the L-phantom with PTV and OAR, with the common beam direction while Figure 5.3b shows the three different plans, with the corresponding fields.

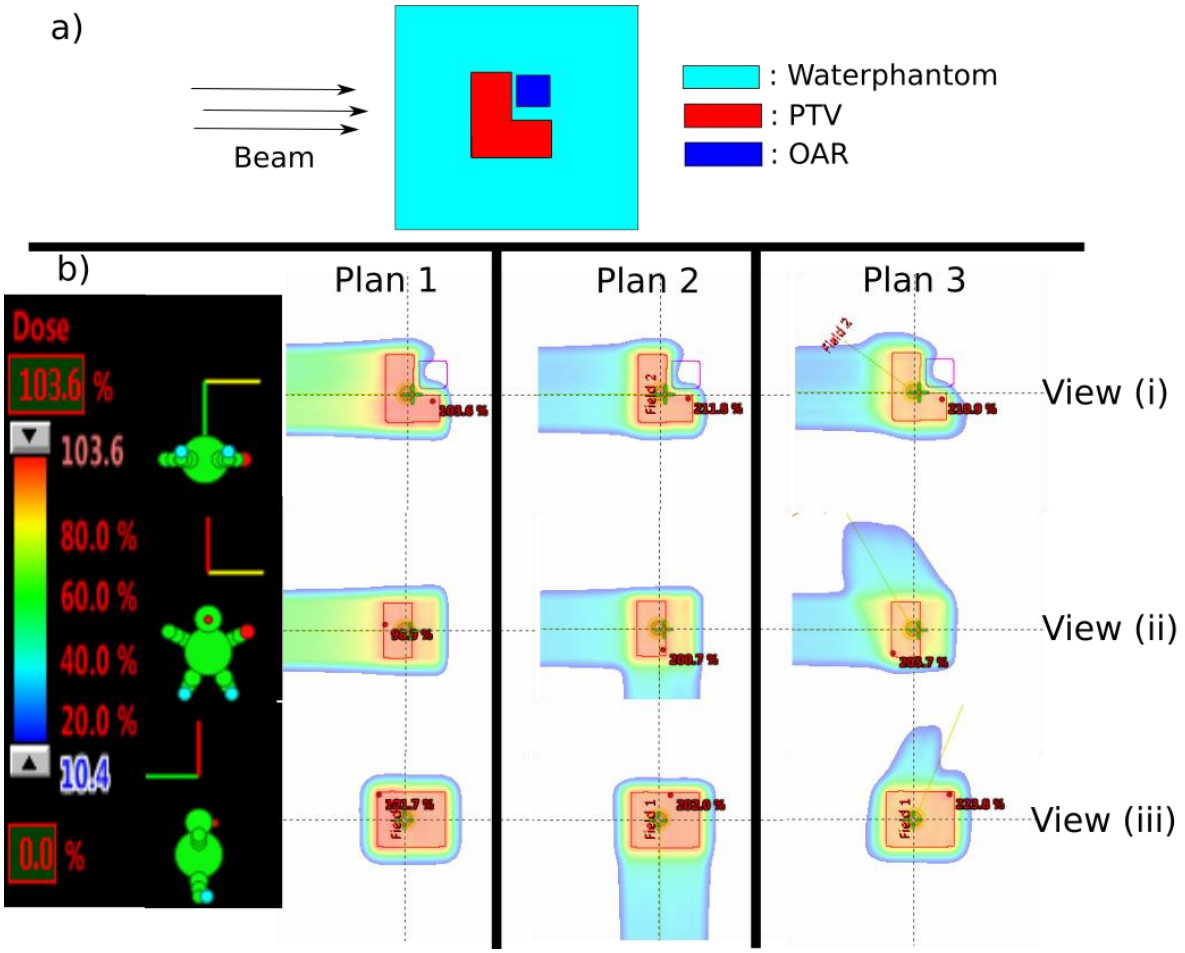

Figure 5.3 a) shows the water phantom, PTV, OAR, and the common beam direction for all plans. The water phantom is given in turquoise, the PTV in red and the OAR in blue. b) The three different plans in three planes, (i) axial, (ii) coronal and (iii) sagittal. The colors indicate the dose level from high (red) to low (blue), as described.

5.3.3 Patient plan

A patient case was also included in this study. The case was a pituitary adenoma and the original plan was optimized to give a homogenous dose of 54 Gy(RBE) to the PTV, with 1.8 Gy(RBE) in each fraction The original plan was an IMRT plan, meaning a homogenous RBE-weighted dose were not given by each field, but by the sum of the two fields. It was therefore of interest to optimize only one of the field and compare to the original plan. The re-optimization was done with respect to the WED model and $RBE_{1.1}$. The original treatment plan, with an illustration of the different fields can be viewed in Figure 5.4. Here the patient is seen from above where the blue outline

represents the PTV. The red arrow represents field 1, and was the field optimized in this project.

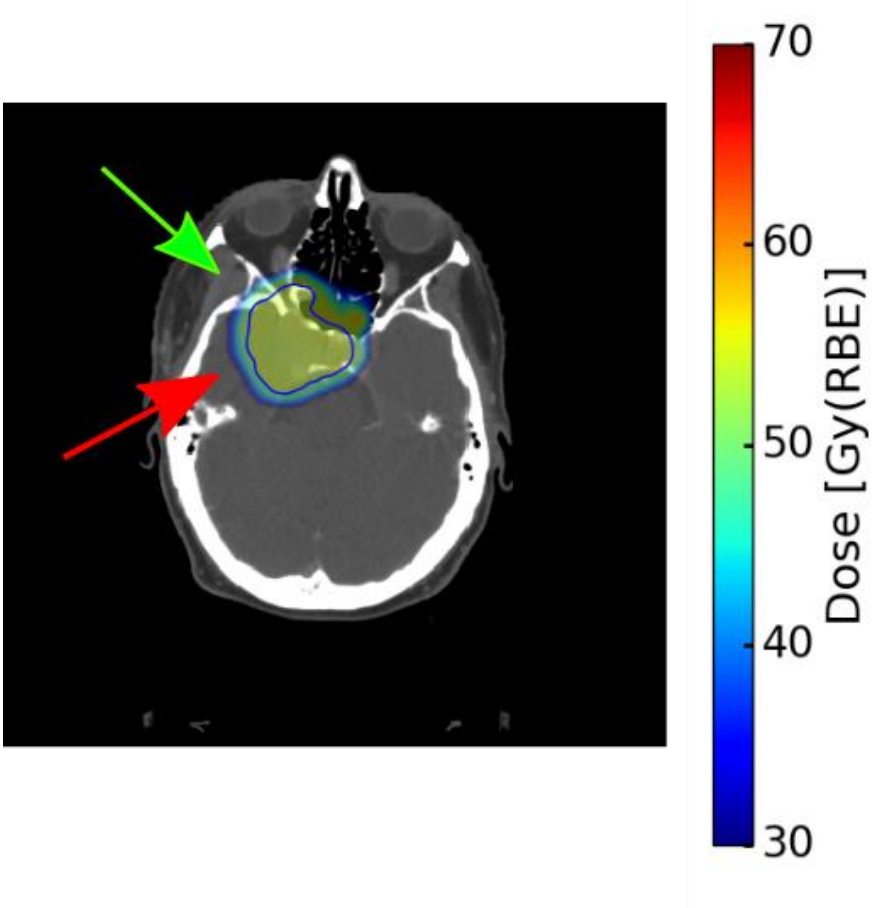

Figure 5.4 Original plan for patient, with the two fields drawn as arrows. Red arrow represents field 1, and green represents field 2. This figure comes from the Eclipse TPS.

5.4 RBE-models

In this project, three variable RBE-models were used; the model by Wedenberg et al. [58] (WED), the model by Unkelbach et al. [50] (UNK), and the non-linear model by Rørvik et al. [44] (ROR). They all model the RBE using LET as input parameters. In addition to these, the WED and ROR use the α_x/β_x for photons as input parameter to account for RBE variations with tissue type. While UNK and WED use the LET_d, ROR

use a non-linear dependency of RBE on LET, and therefore utilize the LET spectrum as input parameter instead of LET_d [50].

The WED suggests that the parameter RBE_{min} equals 1, while the RBE_{max} depends on the $\mathrm{LET_d}$ and the $(\alpha/\beta)_x$ as follows:

$$RBE_{max}(LET_d, (\alpha/\beta)_x) = 1 + \frac{0.434\ \mathrm{Gy(keV/\mu m)^{-1}}}{(\alpha/\beta)_x} LET_d$$
$$RBE_{min} = 1 \tag{5.1}$$

Wedenberg et al. were interested in the linear dependency of the $(\alpha/\beta)_x$ and the LET_d. They studied multiple cell-lines and used linear regression to establish a model.

ROR is based on a non-linear dependency between the RBE and LET. As for the WED, the $\mathrm{RBE_{min}} = 1$, but for the $\mathrm{RBE_{max}}$, ROR is based on a biological weighting function (BWF) which is derived from in vitro cell experiment. The BWF ($r_{max}(L)$) weights the LET-spectrum ($d(L)$). The RBE is written as written as:

$$RBE_{max}(d(L)) = \int_0^\infty r_{max}(L) d(L) dL$$

$$r_{max}(L) = 1 + \frac{\mathrm{Gy}}{(\alpha/\beta)_x}\left(0.578 \left(\frac{\mathrm{keV}}{\mu\mathrm{m}}\right)^{-1} L - 0.0808 \left(\frac{\mathrm{keV}}{\mu\mathrm{m}}\right)^{-2} L^2 + 0.00564 \left(\frac{\mathrm{keV}}{\mu\mathrm{m}}\right)^{-3} L^3 \right. \tag{5.2}$$
$$\left. - 9.92 \times 10^{-5} \left(\frac{\mathrm{keV}}{\mu\mathrm{m}}\right)^{-4} L^4\right), \qquad L < 37.0\ \mathrm{keV/\mu m}$$

$$RBE_{min} = 1$$

UNK is not an explicit biological model for RBE calculation, but primarily a model for LET optimization. It is based on the principle of an RBE which is linear dependent of the LET, and a mean RBE of 1.1 across the SOBP. The RBE can therefore be formulated as:

$$RBE = 1 + 0.04(keV/\mu m)^{-1} LET_d \tag{5.3}$$

By setting $RBE_{max} = RBE_{min} = RBE = 1 + 0.04(keV/\mu m)^{-1} LET_d$, a RBE model in our formalism is created. In contrast to ROR and WED, UNK is not fitted to *in vitro* data to find the absolute RBE value, and is independent of dose.

The cell-line used in this project is V79, also used by Wilkens [59], which gives an $(\alpha/\beta)_x = 3.76$.

6. Results

6.1 Cubic PTV in water

Figure 6.1 shows the dose distribution for each model after optimization of their respective RBE-weighted plan, on a plane in the center of the PTV. The plot shows that for all variable RBE models, the PTV receives a reasonable homogenous RBE-weighted dose of 2 Gy(RBE). This can also be seen from Figure 6.3 where the solid lines indicate the distribution of biological dose in the PTV. This shows that the dose to the PTV was between 1.9 and 2.1 Gy(RBE) for the whole PTV. These results indicate that the plans have been correctly optimized with all RBE models.

A comparison between the physical dose of the plan optimized with constant RBE of 1.1 and with the plans optimized with variable RBE-models can be seen in Figure 6.2. The physical dose from the variable RBE optimized plans (shown in the left column of the figure) has been subtracted from the physical dose from $\mathrm{RBE}_{1.1}$ plan (top row). The dose difference (right column) indicates that the physical dose for the variable RBE-models are generally lower than with $\mathrm{RBE}_{1.1}$.

In addition to the RBE-weighted DVHs, Figure 6.3 also shows the DVHs for their corresponding physical doses (dashed lines). While RBE-weighted doses are very similar, we can observe clear variations in the physical doses. The dose from the WED optimized plan is the overall lowest physical dose, indicating that this model predicts the highest RBE. On the other hand, the plan optimized with $\mathrm{RBE}_{1.1}$ gives the highest dose. The mean, minimum and maximum physical and RBE-weighted dose for the PTV is included in Table 6.1.

The plots from the optimizer can be found in Appendix D .

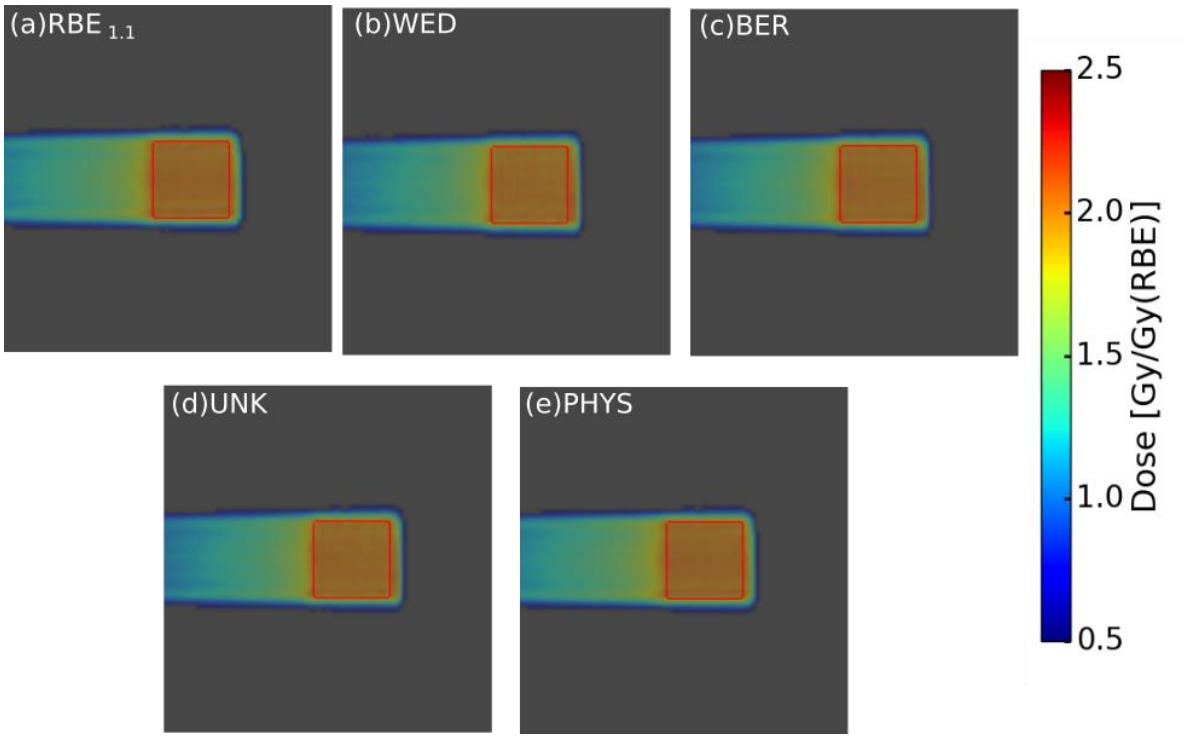

Figure 6.1 RBE weighted dose distributions for different biological models (a-d) and physical dose distribution (e) for the plan optimized only with respect to physical dose. All plans are optimized for 2 Gy(RBE) for RBE models and 2 Gy for the physical dose.

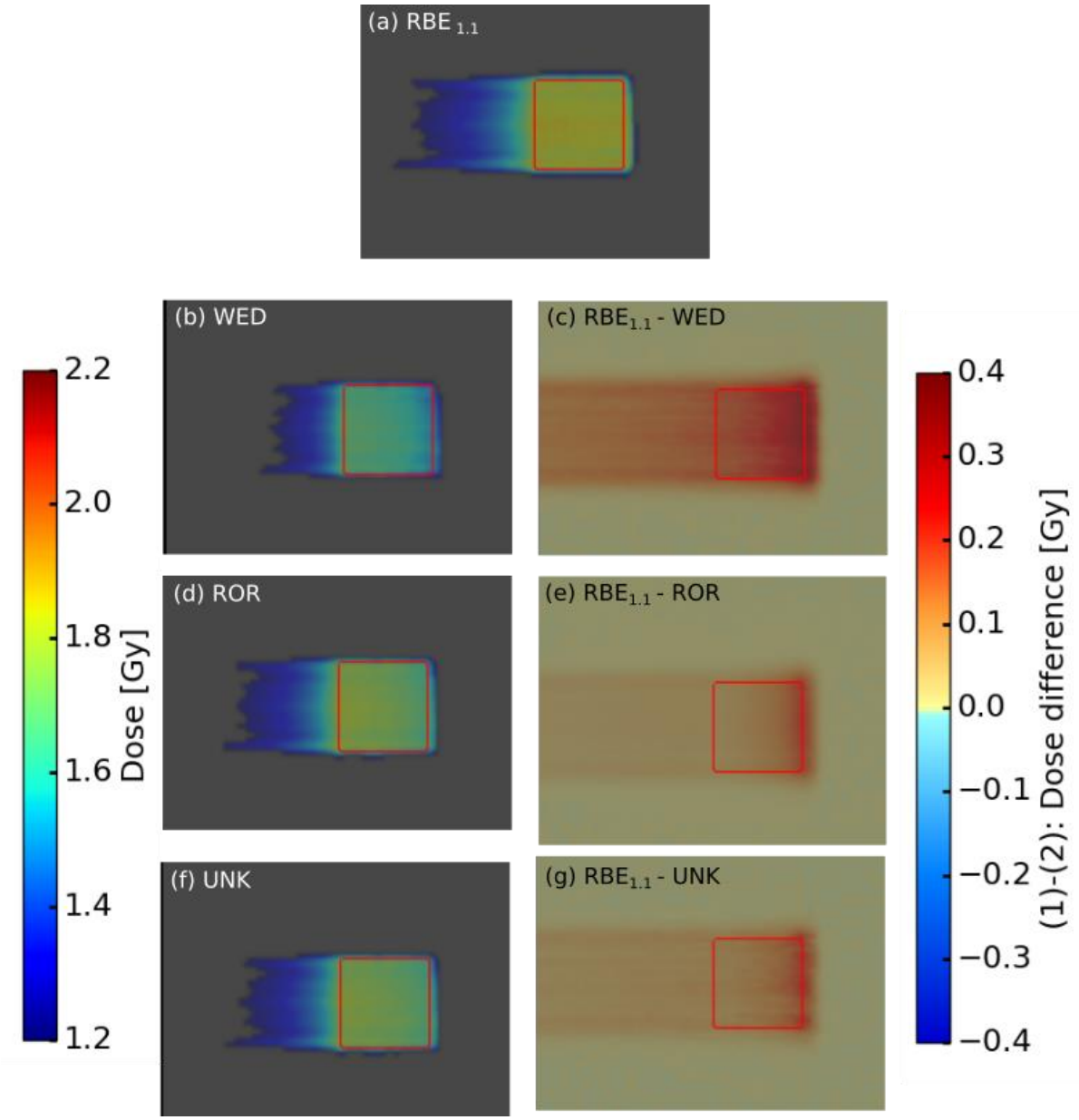

Figure 6.2 Comparison of the physical dose from plans optimized with a variable RBE model and constant RBE. The plots b,d and f show the RBE-weighted dose, while the c,e and g show the difference compared to the $RBE_{1.1}$ optimized plan. Dose below 1.2 Gy is set as transparent (left plots), while dose differences (right plots) are only shown between -0.4 Gy and 0.4 Gy.

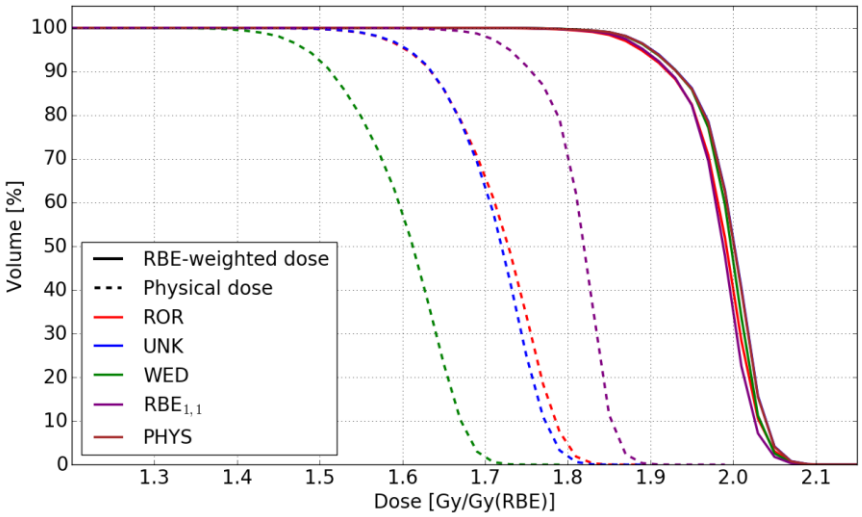

Figure 6.3 DVHs of RBE-weighted dose (solid lines), and respective physical dose (dotted lines) for the plans optimized with respect to RBE-weighted dose. A DVH for the plan optimized with respect to physical dose is also given as PHYS. The metrics for the physical doses and RBE-weighted doses is given in Table 6.1.

Table 6.1 Dose metrics for RBE-weighted doses in Figure 6.3. The corresponding physical doses are given in parenthesis.

Model	**Mean dose [Gy(RBE)] ([Gy])**	**Min dose [Gy(RBE)] ([Gy])**	**Max dose [Gy(RBE)] ([Gy])**
WED	1.98 (1.60)	1.61 (1.23)	2.13 (1.75)
$RBE_{1.1}$	1.99 (1.81)	1.64 (1.50)	2.11 (1.92)
UNK	1.98 (1.71)	1.61 (1.34)	2.13 (1.85)
ROR	1.99 (1.72)	1.64 (1.35)	2.13 (1.86)

1-D plots of the comparison of the physical doses from the RBE models are presented along the beam direction in Figure 6.4 and lateral direction in Figure 6.5. For the depth-dose plot, three different positions on the SOBP have been marked, and the different values can be found in Table 6.2 It is apparent that the biological dose is approximately 2 Gy(RBE) along the entire depth from 13-17cm in water for all plans. It can also be seen that the physical dose to the respective RBE-weighted models is generally lower

compared to the biological dose, i.e. the RBE is above 1, which is expected. The physical dose from the variable RBE-models have similar shape, and while the WED gives the lowest physical dose of these, UNK and ROR model deliver slightly higher and similar physical dose.

A comparison of the biological doses for a plan optimized for physical dose was also made and is presented in Figure 6.6. There it can be seen that the shape of the biological dose for the variable RBE-models is similar but vary in magnitude. The RBE-weighted dose from WED is higher the two other models, while UNK is higher again than ROR. This result is not the same as previously seen, as UNK and ROR is observed to be similar in physical dose distribution when optimized with respect to RBE-weighted dose.

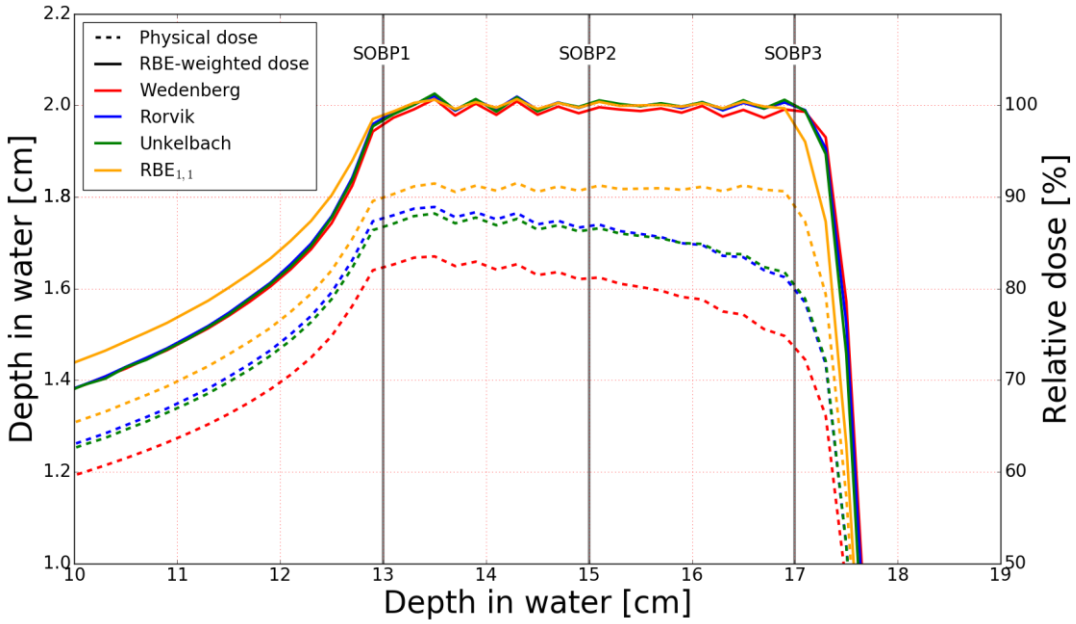

Figure 6.4 Physical dose (dashed lines), for the different plans optimized with respect to RBE-weighted dose (solid lines) in depth dose direction. Three different areas of the SOBP is marked, and their respective values are given in Table 6.2.

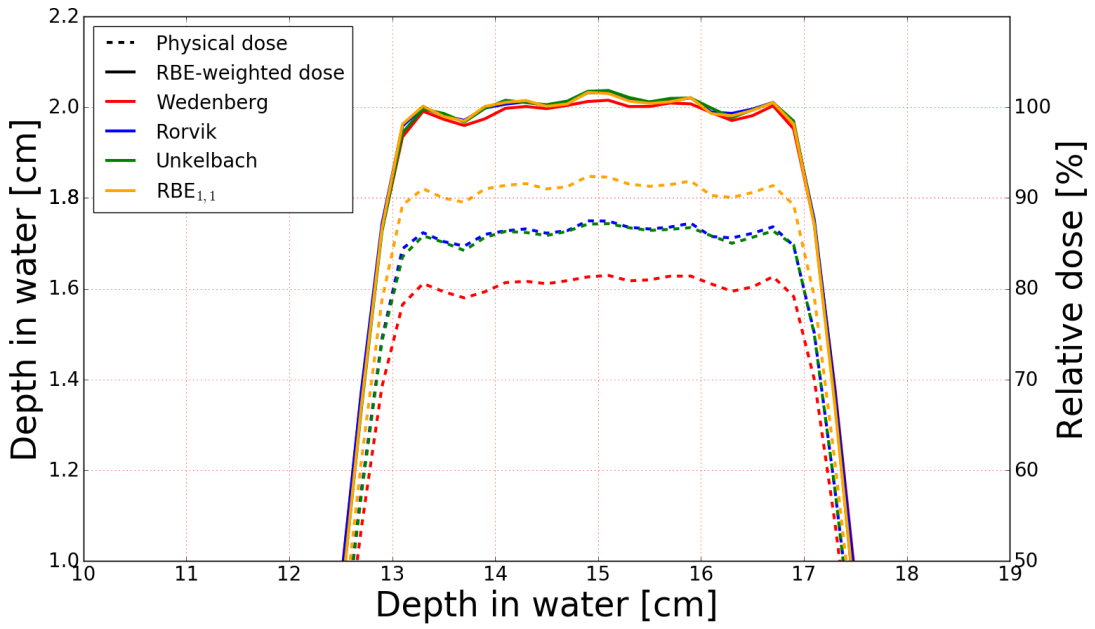

Figure 6.5 Physical dose (dashed lines), for the different plans optimized with respect to RBE-weighted dose (solid lines) in lateral direction.

Table 6.2 Physical dose in different regions in the depth dose profiles for the four biological dose plans given in Figure 6.4 at three locations along the SOBP. The percent values in the parenthesis are the physical dose compared to the $RBE_{1.1}$ plan.

Dose (Gy)	**Region**		
Model	**SOBP1**	**SOBP2**	**SOBP3**
$RBE_{1.1}$	1.80	1.82	1.79
WED	1.65 (92 %)	1.62 (89 %)	1.48 (83 %)
ROR	1.76 (98 %)	1.74 (96 %)	1.61 (90 %)
UNK	1.74 (97 %)	1.73 (95 %)	1.61 (90 %)

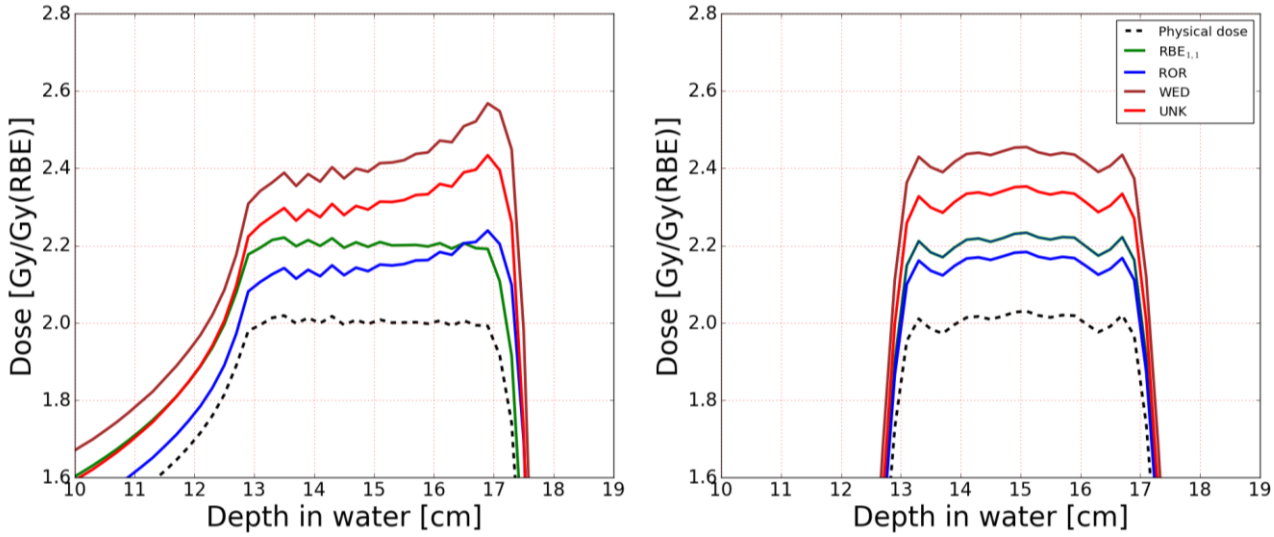

Figure 6.6 Comparison of RBE-weighted dose of a plan optimized with respect to physical dose of 2Gy in beam direction (left) and lateral direction (right).

6.2 The L-PTV in water

6.2.1 Single field plan

Figure 6.7 shows the RBE-weighted dose distributions for the single field plan. It can be observed that the PTV (outlined in red), received a homogenous dose of approximately 2 Gy(RBE) for all models. As for the cubical PTV, this indicates again the correctness of the optimization process for all models. It can also be seen that the OAR (outlined in pink), receives a small dose at the edge closest to the PTV. The same results can also be seen from the DVHs (Figure 6.9). The dose metrics (Table 6.3 and Table 6.4), also shows that the minimum RBE-weighted dose varied between 1.63 and 1.83 Gy(RBE), while the maximum RBE-weighted dose were between 2.14 – 2.23 Gy(RBE).

Figure 6.8 shows the physical doses from the respective RBE models and the difference between the $RBE_{1.1}$ dose and the variable RBE models. It can be observed that the physical dose from the variable RBE-models is lower than for the plan with constant RBE, with the highest differences at the distal end of the beam. This is also indicated

by the DVHs (Figure 6.9), and the belonging DVH metrics (Table 6.3 and Table 6.4), where the mean physical dose to both the PTV and OAR for the variable RBE-models are smaller than for the $RBE_{1.1}$ plan. This is similar as dose distribution to the cubical PTV. The plots from the optimizer can be found in Appendix D .

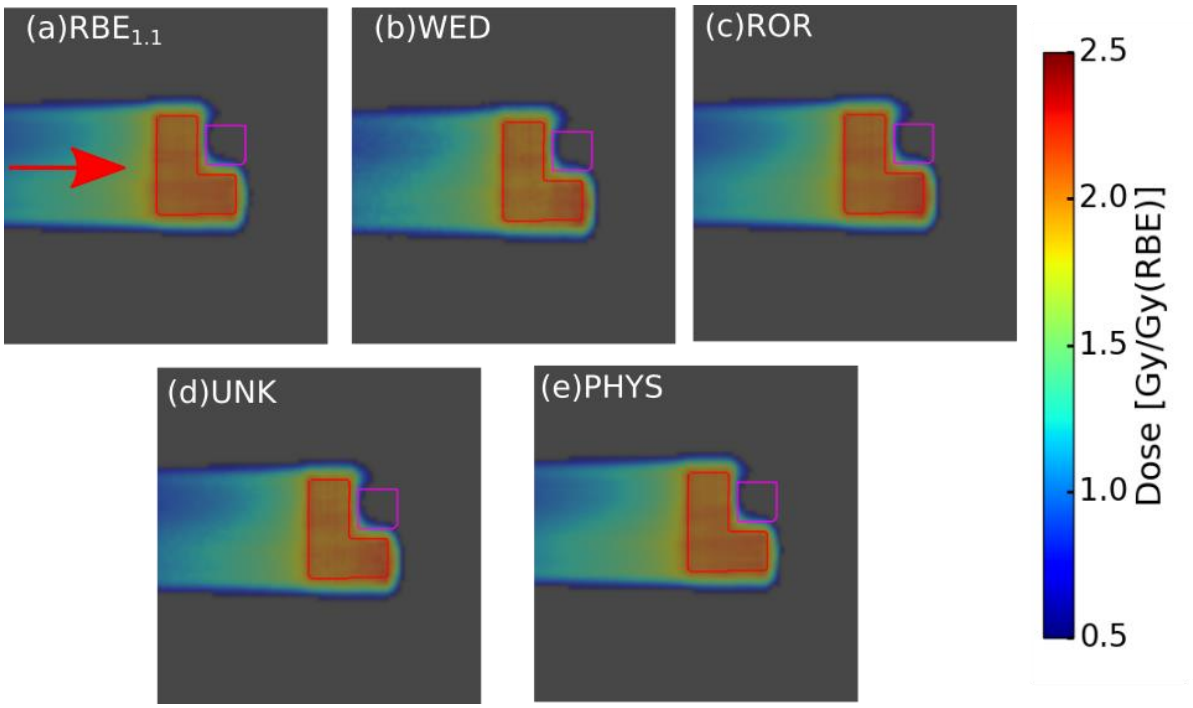

Figure 6.7 RBE weighted dose distributions for different biological models (a-d) and physical dose distribution (e) for the plan optimized only with respect to physical dose. All plans are optimized for 2 Gy(RBE) for RBE models and 2 Gy for the physical dose. The PTV is outlined in red and the OAR is outlined in pink. The red arrow shows the beam direction.

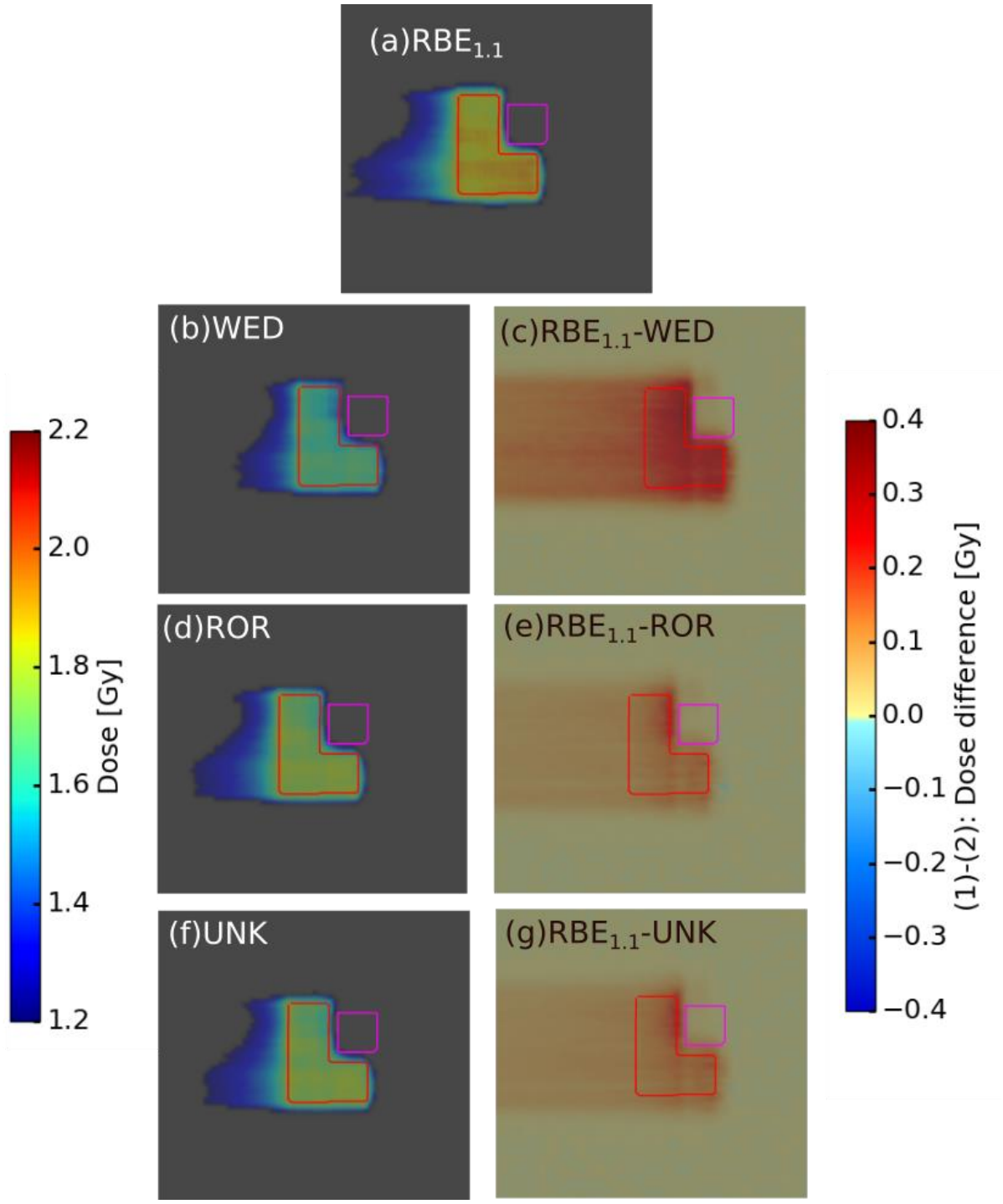

Figure 6.8 Comparison of the physical dose distributions from a plans optimized with a variable RBE model and constant RBE. The plots b,d and f show the RBE-weighted dose, while the c,e and g show the difference compared to the $RBE_{1.1}$ optimized plan (a). Dose below 1.2 Gy is set as transparent (left plot), while dose differences (right plot) only show between 0.4 Gy and -0.4 Gy.

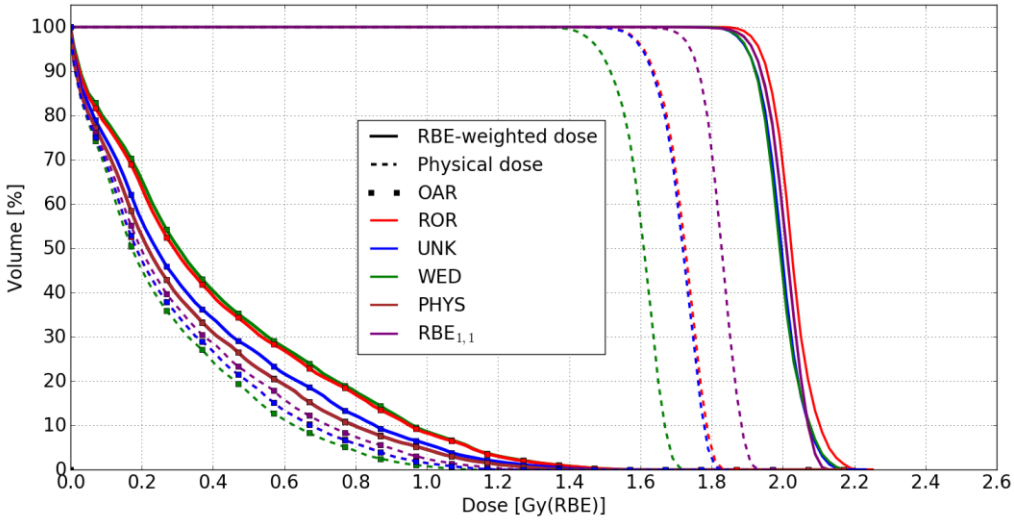

Figure 6.9 DVHs of RBE-weighted dose (solid lines), and respective physical dose (dotted lines) for the plans optimized with respect to RBE-weighted dose. The lines marked with squares represents the RBE-weighted dose and the physical dose the OAR. The PTV and OAR metrics for the physical doses and RBE-weighted doses is given in Table 6.3 and Table 6.4.

Table 6.3 DVH metrics for the L-PTV plan with a single field. The table displays the RBE-weighted doses belonging to the PTV, and the belonging physical doses in parenthesis.

Model	Mean dose [Gy(RBE)] ([Gy])	Min dose [Gy(RBE)] ([Gy])	Max dose [Gy(RBE)] ([Gy])
WED	1.99 (1.60)	1.78 (1.30)	2.21 (1.73)
$RBE_{1.1}$	2.01 (1.82)	1.63 (1.48)	2.14 (1.94)
UNK	1.96 (1.71)	1.76 (1.39)	2.19 (1.83)
ROR	2.03 (1.72)	1.83 (1.43)	2.23 (1.85)
PHYS	2.01	1.65	2.14

Table 6.4 DVH metrics for the L-PTV plan with a single field. The table displays the RBE-weighted doses belonging to the OAR and the belonging physical doses in parenthesis.

Model	Mean dose [Gy(RBE)] ([Gy])	Min dose [Gy(RBE)] ([Gy])	Max dose [Gy(RBE)] ([Gy])
WED	0.42 (0.26)	0.002 (0.001)	1.64 (1.20)
$RBE_{1.1}$	0.32 (0.29)	0.001 (0.001)	1.45 (1.36)
UNK	0.35 (0.28)	0.001 (0.001)	1.56 (1.28)
ROR	0.41 (0.28	0.001 (0.001)	1.63 (1.29)
PHYS	0.32	0.001	1.49

6.2.2 Two perpendicular fields

Figure 6.10 shows the biological dose for the treatment plan with two perpendicular fields. It can be observed that the PTV (marked red), receives a homogenous dose of 2 Gy(RBE), while the OAR (marked pink) receives a small dose at the edge close to the PTV. This is also supported by Figure 6.12, which shows a DVH for the PTV and for the OAR, and the belonging RBE-weighted and physical doses. There it can be see that the median dose lies around 2 Gy(RBE), while the OAR receives a maximum of 1.2 Gy(RBE), dependent on the model. This is also seen in the belonging dose metrics in Table 6.5, which gives the mean dose for the DVH to be approximately 2 Gy(RBE) for the RBE-weighted doses, and 2 Gy for the plan optimized with respect to physical dose.

Figure 6.11 shows the physical dose distributions (a,b,d and f) belonging to the RBE-weighted dose plans and the dose difference (c,e and g) between the variable RBE models and the plan with constant RBE of 1.1. It can be observed that the physical dose from the variable RBE models are lower than for the $RBE_{1.1}$, and the difference is evenly distributed over the PTV, contrary to the dose distribution from the single field L-PTV and cubic PTV. The difference is also supported by the DVH (Figure 6.12), and the metrics for physical doses to both PTV and OAR (Table 6.5 and Table 6.6), which suggest lowest physical dose from WED, while UNK and ROR are similar. The plots from the optimizer can be found in Appendix D .

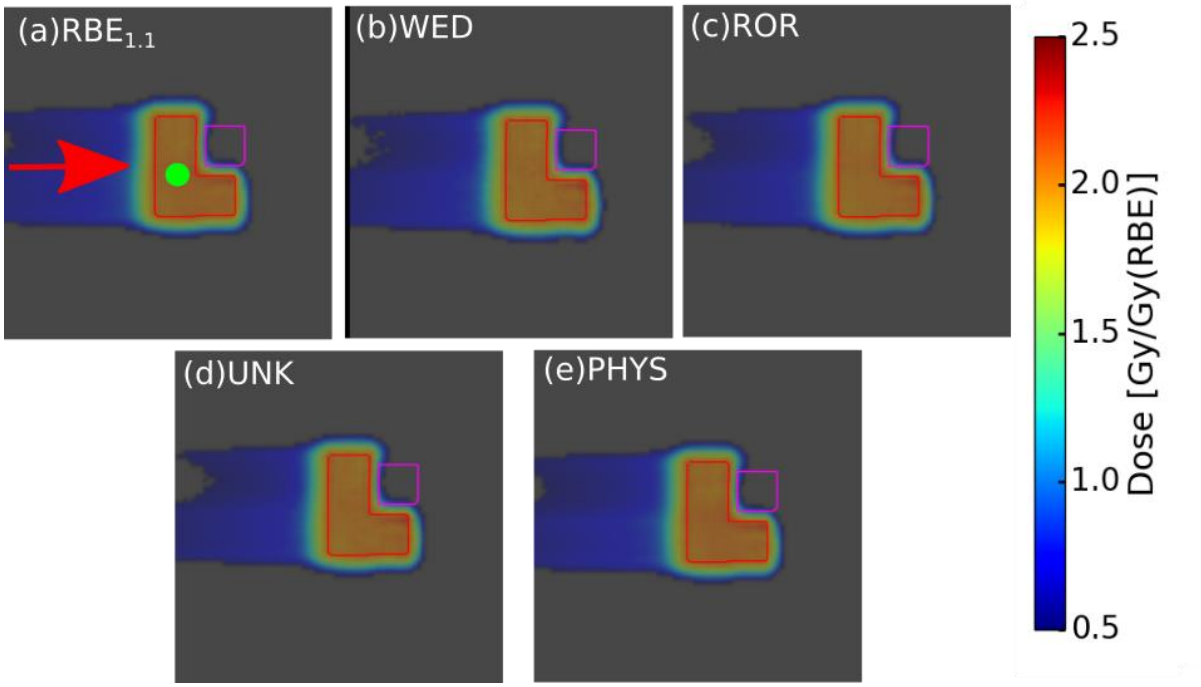

Figure 6.10 RBE weighted dose distributions for different biological models (a-d) and physical dose distribution (e) for the plan optimized only with respect to physical dose. All plans are optimized for 2 Gy(RBE) for RBE models and 2 Gy for the physical dose. The PTV and OAR are outlined in red and pink, respectively. The red arrow shows the direction of the first field, while the green dot shows the direction of the second field (into the plane).

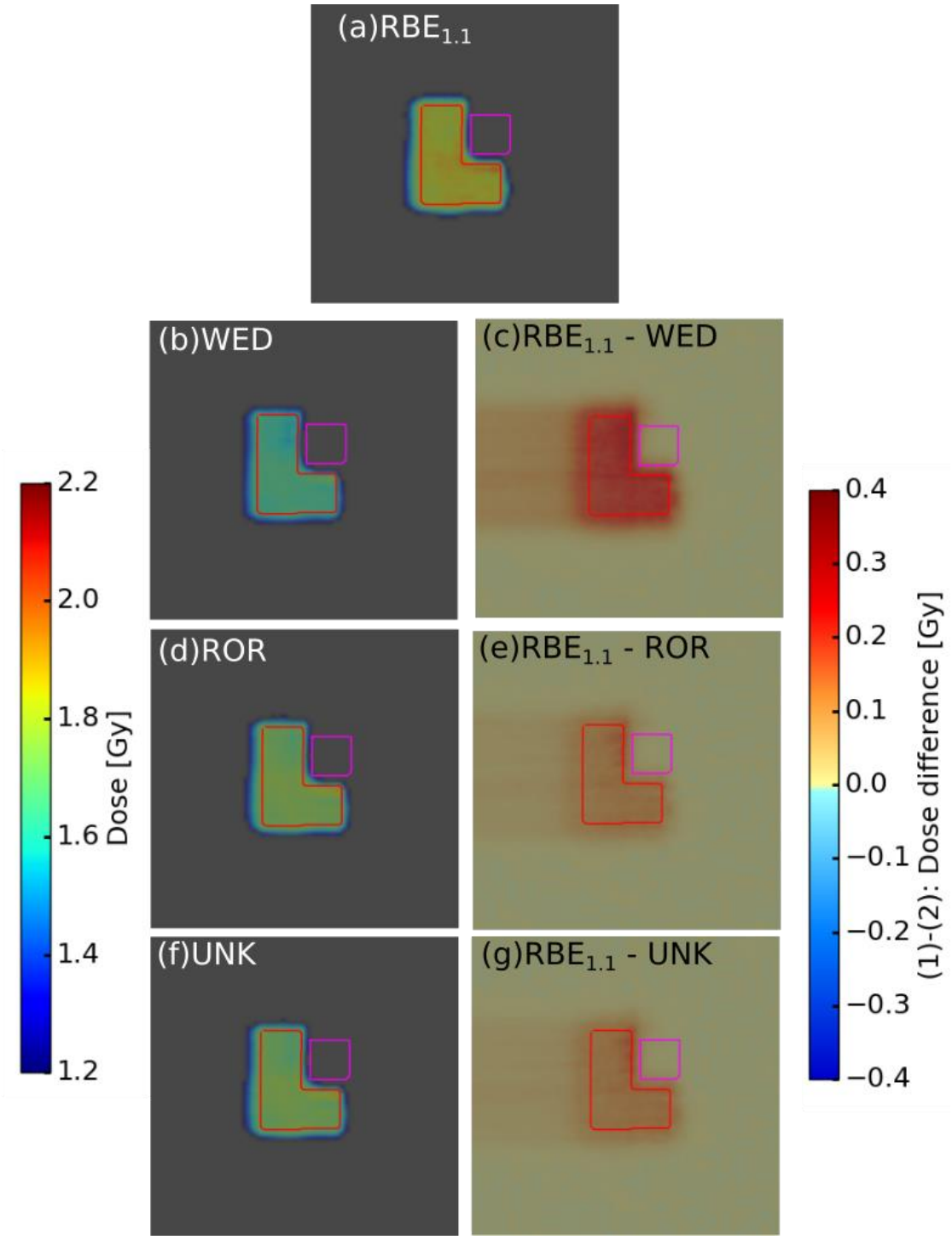

Figure 6.11 Comparison of the physical dose distributions from a plans optimized with a variable RBE model and constant RBE. The plots b,d and f show the RBE-weighted dose, while the c,e and g shows the difference compared to the $RBE_{1.1}$ optimized plan (a). Dose below 1.2 Gy is set as transparent (left plot), while dose differences (right plot) only show between 0.4 Gy and -0.4 Gy.

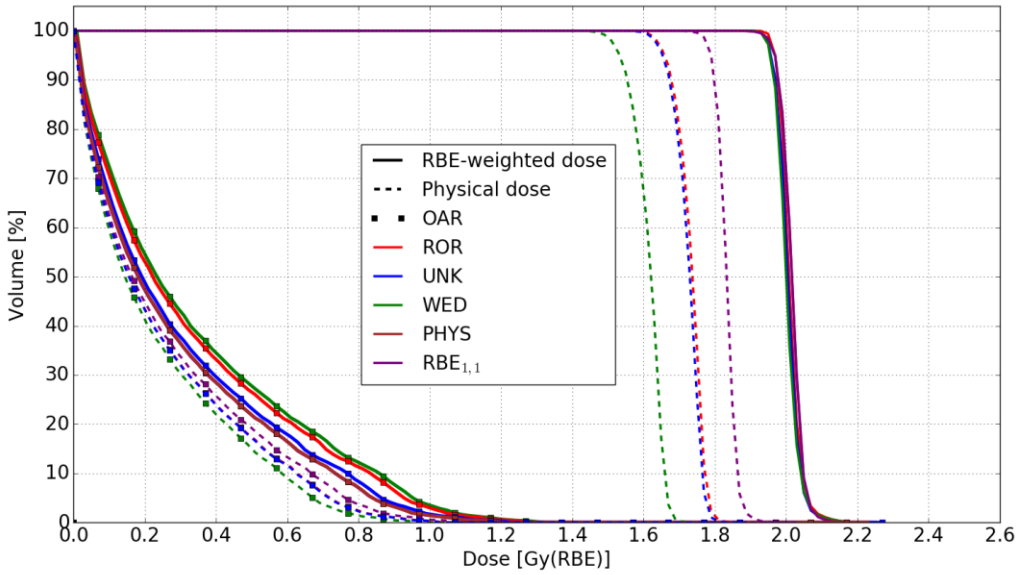

Figure 6.12 DVHs of RBE-weighted dose (solid lines), and respective physical dose (dotted lines) for the plans optimized with respect to RBE-weighted dose. The lines marked with squares represents the RBE-weighted dose and the physical dose the OAR. The PTV and OAR metrics for the physical doses and RBE-weighted doses is given in Table 6.5 and Table 6.6.

Table 6.5 Dose metrics for the L-PTV plan with two perpendicular fields. The table displays the RBE-weighted doses belonging to the PTV, and their respective physical doses in parenthesis.

Model	**Mean dose [Gy(RBE)] ([Gy])**	**Min dose [Gy(RBE)] ([Gy])**	**Max dose [Gy(RBE)] ([Gy])**
WED	2.00 (1.61)	1.88 (1.40)	2.20 (1.74)
$RBE_{1.1}$	2.02 (1.83)	1.83 (1.66)	2.18 (1.98)
UNK	2.01 (1.72)	1.88 (1.52)	2.22 (1.86)
ROR	2.01 (1.73)	1.91 (1.54)	2.21 (1.86)
PHYS	2.02	1.84	2.19

Table 6.6 Dose metrics for the L-PTV plan with two perpendicular fields. The table displays the RBE-weighted doses belonging to the OAR, and their respective physical doses in parenthesis.

Model	Mean dose [Gy(RBE)] ([Gy])	Min dose [Gy(RBE)] ([Gy])	Max dose [Gy(RBE)] ([Gy])
WED	0.34 (0.24)	0.002 (0.001)	1.42 (1.06)
$RBE_{1.1}$	0.28 (0.26)	0.001 (0.001)	1.31 (1.19)
UNK	0.30 (0.24)	0.002 (0.001)	1.34 (1.12)
ROR	0.33 (0.24)	0.002 (0.001)	1.39 (1.13)
PHYS	0.29	0.001	1.32

6.2.3 Two angular fields

Figure 6.13 shows the biological dose distribution for the treatment plan with two angular fields. There it can be seen that most of the PTV (marked red), receives a RBE-weighted dose of 2 Gy(RBE). This is supported by the DVH in Figure 6.15, which displays the DVH of the PTV and OAR. It can be observed that the minimum dose for the PTV is around 1.5 Gy(RBE) which is the lowest for all water phantom plans. The maximum RBE-weighted dose to the OAR is around 1.4 Gy(RBE), which is the highest of all the three L-PTV plans.

Figure 6.14 shows the difference between in physical dose distribution between the variable RBE models and $RBE_{1.1}$. The results are quite similar as for the two other L-PTV plans, where the dose from WED is lower than from ROR and UNK. This is also supported by the DVH (Figure 6.15) and dose metrics (Table 6.7 and Table 6.8). The largest difference is observed at the distal end of the PTV similar to the single fields plan for the L-PTV and the cubic PTV. The plots from the optimizer can be found in Appendix D

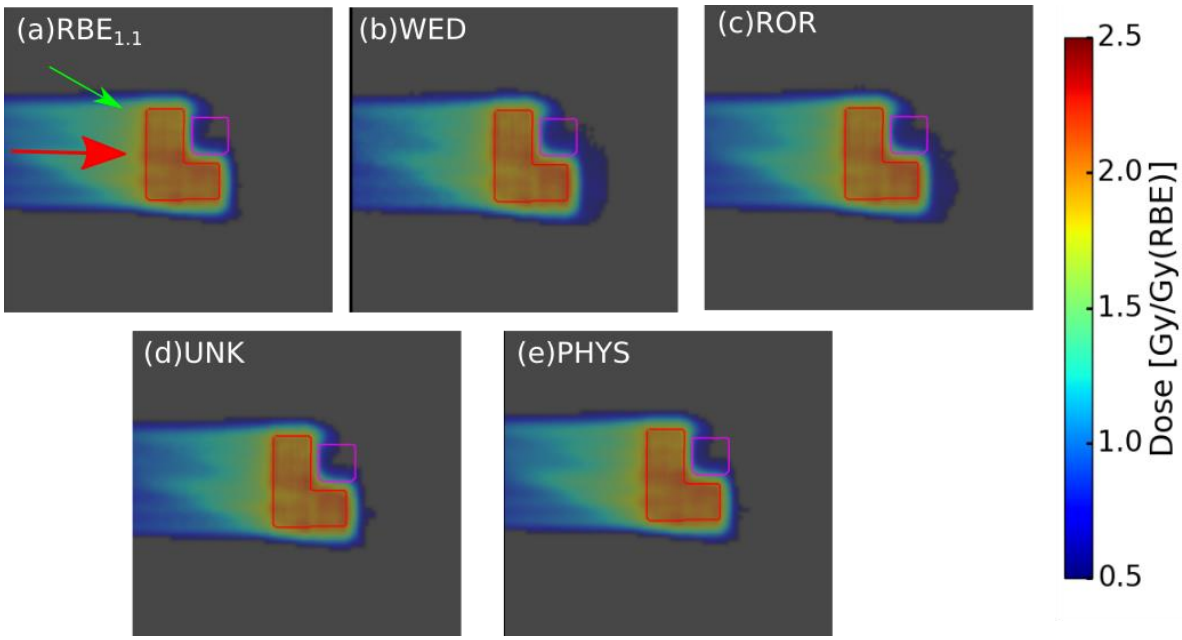

Figure 6.13 RBE weighted dose distributions for different biological models (a-d) and physical dose distribution (e) for the plan optimized only with respect to physical dose. All plans are optimized for 2 Gy(RBE) for RBE models and 2 Gy for the physical dose. The PTV and OAR are outlined in red and pink, respectively. The red arrow shows the first field, while the green arrow shows the second field. Note that the second field also comes through the plane.

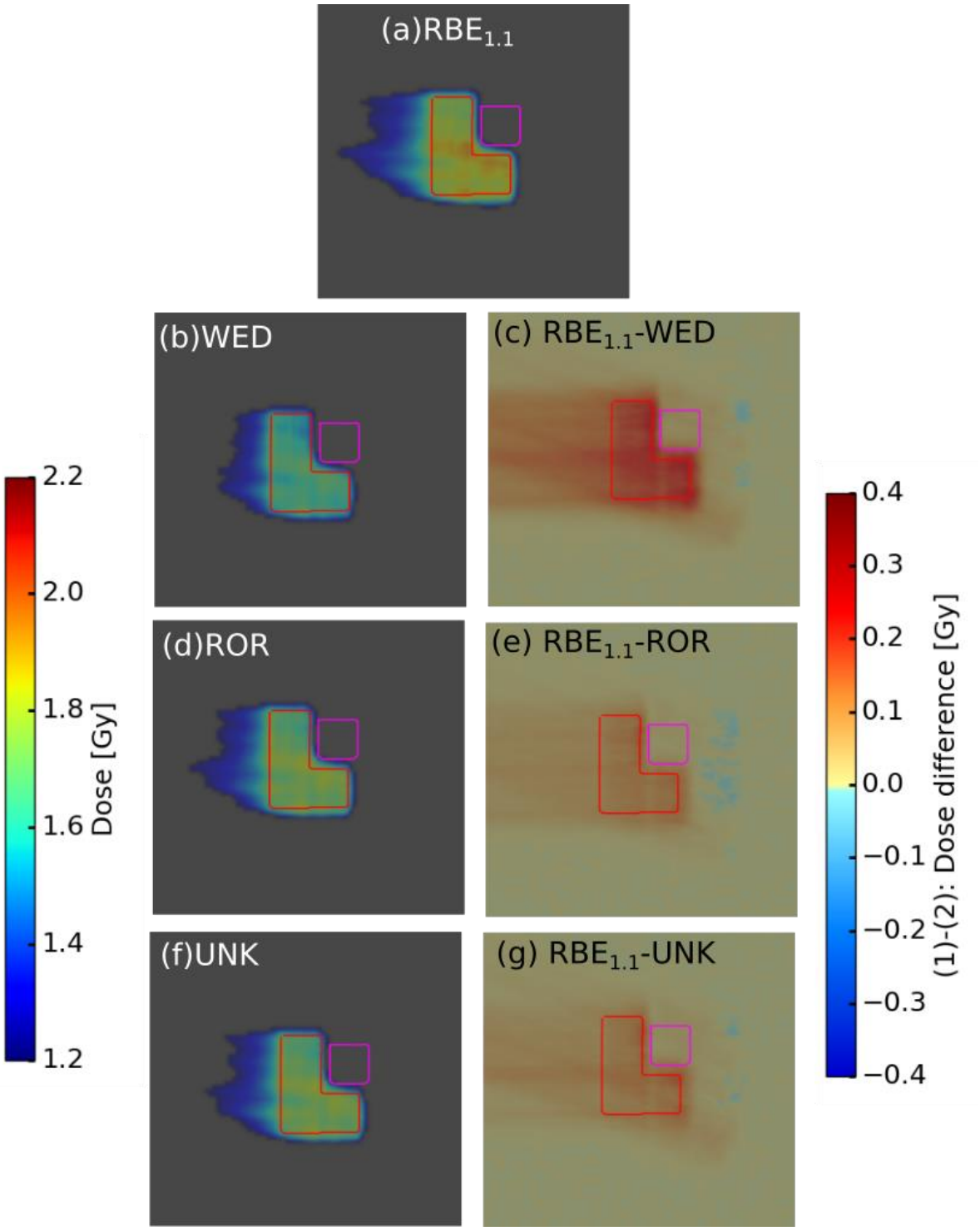

Figure 6.14 Comparison of the physical dose distributions from a plans optimized with a variable RBE model and constant RBE. The plots b,d and f show the RBE-weighted dose, while the c,e and g shows the difference compared to the $RBE_{1.1}$ optimized plan (a). Dose below 1.2 Gy is set as transparent (left plot), while dose differences (right plot) only show between -0.4 Gy and 0.4 Gy.

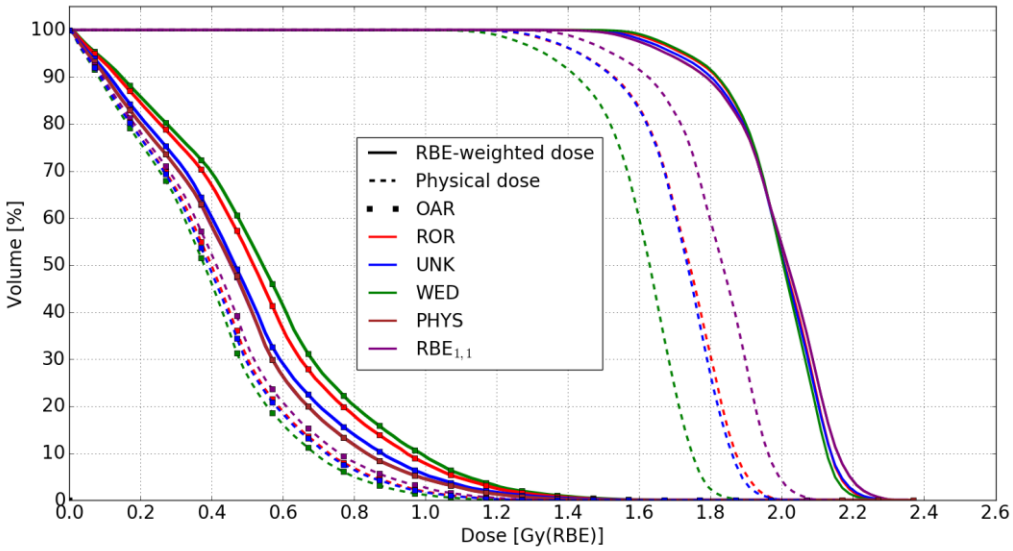

Figure 6.15 DVH of the different biological models for the plan with two angular fields. Solid lines represent the PTV while the dotted lines represents the OAR. The dose metrics can be found in Table 6.7 and Table 6.8.

Table 6.7 Dose metrics for the L-PTV plan with two angular fields. The table displays the RBE-weighted doses belonging to the PTV, and their respective physical doses in parenthesis.

Model	**Mean dose [Gy(RBE)]([Gy])**	**Min dose [Gy(RBE)]([Gy])**	**Max dose [Gy(RBE)]([Gy])**
WED	1.99 (1.61)	1.39 (0.97)	2.27 (1.90)
$RBE_{1.1}$	1.99 (1.81)	1.27 (1.15)	2.33 (2.12)
UNK	1.99 (1.71)	1.30 (1.05)	2.32 (2.02)
ROR	1.99 (1.72)	1.36 (1.05)	2.28 (2.02)
PHYS	1.99	1.28	2.33

Table 6.8 Dose metrics for the L-PTV plan with two angular fields. The table displays the RBE-weighted doses belonging to the OAR, and their respective physical doses in parenthesis.

Model	**Mean dose [Gy(RBE)]([Gy])**	**Min dose [Gy(RBE)]([Gy])**	**Max dose [Gy(RBE)]([Gy])**
WED	0.56 (0.38)	0.008 (0.004)	1.65 (1.25)
$RBE_{1.1}$	0.46 (0.42)	0.005 (0.005)	1.51 (1.38)
UNK	0.48 (0.40)	0.005 (0.004)	1.59 (1.33)
ROR	0.53 (0.41)	0.006 (0.004)	1.62 (1.33)
PHYS	0.46	0.005	1.51

6.2.4 Patient plan

Figure 6.16 shows the original $RBE_{1.1}$ dose distribution for field 1 of the patient plan (a), as well as the two plans optimized with respect to $RBE_{1.1}$ (b) and WED (c). The fields are normalized to visualize the homogenity of the fields, and not to absolute dose, meaning the doses viewed are only for illustrational purposes. It can be seen that the original field is inhomogenous and that the dose is not only deposited in the PTV (outlined in blue); the original plan has a hotspot below the PTV. For the two optimized plans, the dose distribution is more even than for the original plan, but also results in dose outside the PTV. The optimized plans also have a hotspot of dose similar to the original plan outside the PTV. The results indicates that the optimizer works for a patient plan, but there are problems that needs to be solved.

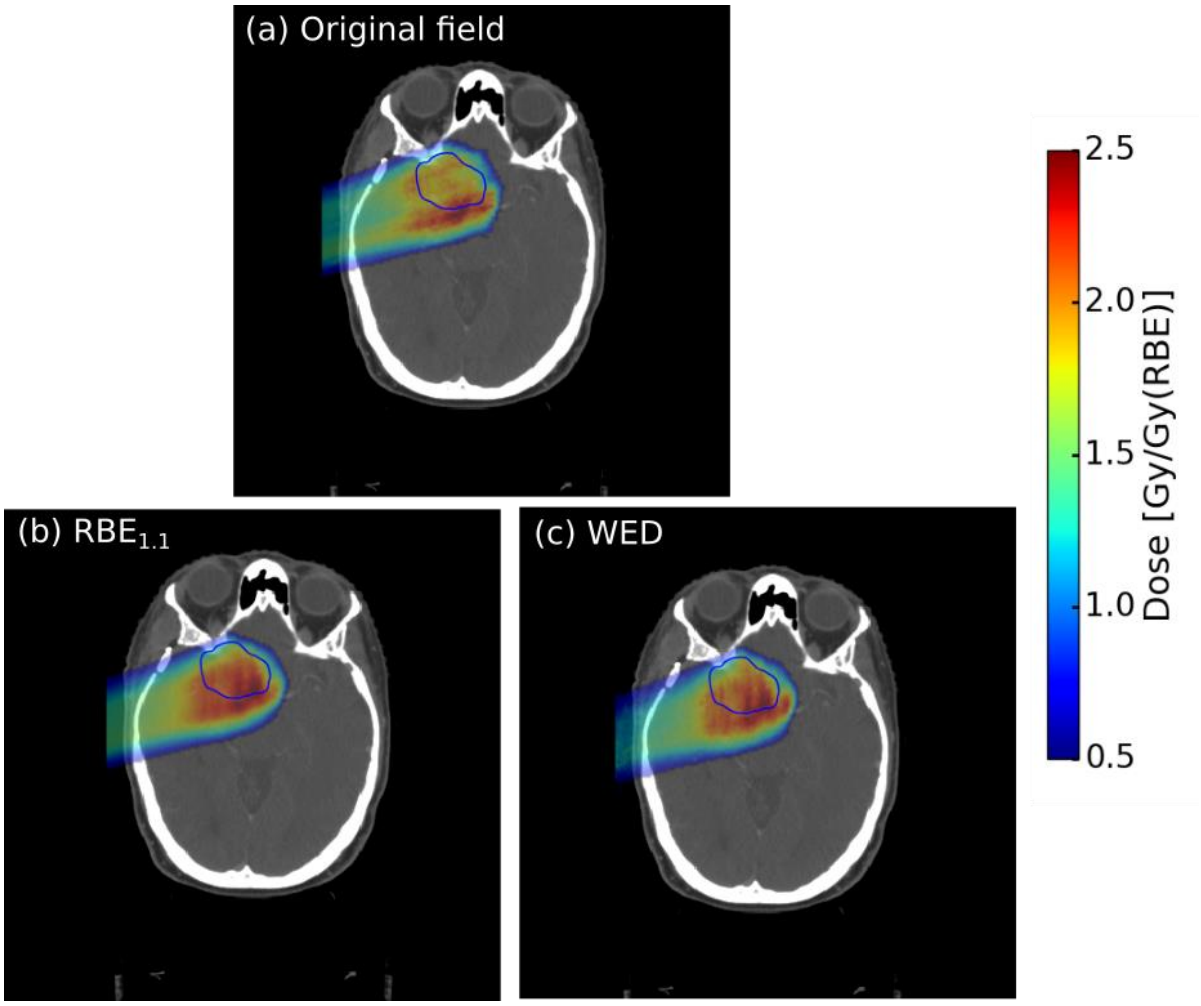

Figure 6.16 Comparison of dose distribution for the original plan for field 1 (a), and the two optimized plans (b and c). Note that these fields are normalized to look at homogeneity in the dose distribution and not according absolute dose level.

7. Discussion

In this project, a prototype optimizer has been used together with the FLUKA MC-code to re-optimize treatment plans with respect to different RBE-models. A thorough method has been made for the use of the optimizer, and the optimized results have been verified for four different plans; one for a cube-shaped target in a water and three for an L-shaped target in water. A single field uniform dose (SFUD) optimization of a patient plans has also been done. The dose distributions of the different treatment plans have been compared, with respect to the physical dose. The results indicate that for all treatments plans, the PTV achieved the prescribed RBE-weighted dose of 2 Gy(RBE) for all biological models, which indicates that the optimizer works well as no errors were observed for either of the phantoms.

The general trend showed that the WED model provided the lowest physical dose, while UNK and ROR provided similar dose distributions to the PTV. The WED model resulted in a physical dose which was generally 11% lower than the physical dose from plans optimized with $RBE_{1.1}$, while UNK and ROR was about 6% lower. The general problems that occurred and was solved during this project consisted of making the in-house dose verification tool compatible with the requirements of the optimizer and vice-versa.

7.1 Optimization process

For the cube-shaped water phantom, the treatment plans optimized with both RBE-weighted dose and physical dose delivered a seemingly homogenous biological dose of 2 Gy(RBE) to the entire volume. This is supported by the DVHs, which suggests a mean dose around 2 Gy(RBE) and 1D plots, which shows a SOBP around 2 Gy(RBE) in the area of the PTV. The optimizer works therefore well with the water phantom.

For the L-phantom, three separate plans were made; one field, two perpendicular fields, and two angular fields. All three were tested with the same biological models as for the

first water phantom. The first plan (one field) was optimized well, and the results showed an even dose of 2 Gy(RBE) for all models. The DVH for this plan is not as good as for the first water phantom, but sufficient as the median biological dose is 2 Gy(RBE). It is not always physical possible to achieve a perfect DVH to the PTV while also sparing the OAR, especially with a single field. A middle-course is often needed in the treatment planning process.

For the plan with two perpendicular fields, the results showed, as with the single field plan, a homogenous RBE-weighted dose of 2 Gy(RBE) to the PTV, and no elevated values in the OAR, which means the optimizer also works well with two fields. The DVH showed better results than for the L-phantom with one field, which was expected as the field positioning in this plan provided a better basis for homogenous dose throughout the PTV.

For the plan with two angular fields, the result showed that most of the PTV received a biological dose of 2 Gy(RBE), while the top of the L, received somewhat less dose. This might come from the unpractical field positioning, as this particular plan was made to test different angles to optimize with and to test the ROI positioning, and not to get the best possible clinical plan. However, the DVH showed a median dose around 2 Gy, which means that most of the PTV received sufficient dose. It can, however, be observed that the minimum dose is around 1.5 Gy(RBE), which is the lowest of the four plans.

By comparing the DVH from the L-phantom plans, with the output from the optimizer, found in Appendix D , it can be seen that the DVHs are similar. This is also an indication that the optimizer works well and the method is functional.

The optimizer was also tested on a patient plan, where one field from the patient plan was optimized to see if better dose distribution could be achieved. The result showed that the dose from field 1 in the original plan was not homogenous, and some of the dose was outside of the PTV. The optimized results showed a more homogenous dose

distribution, although, as also seen in the original field, some of the dose was distributed outside the PTV. The shape of the dose distribution also indicates that the results from the optimizer are shifted, meaning the PTV was misplaced or shifted in the optimizer. Although the results from the patient plan are preliminary, the homogenous dose distribution from the two plans shows the potential of using the optimizer on clinical patient cases.

During this work it appeared that the ROI-files (information about which region to score) had a different rotation than the phantom/patient. As a result, a method for rotating the patient and the ROI-files to orientations corresponding to the new beam directions had to be developed. This problem might arise from the script HUchanger.py, which provides information about the voxel location for the different ROIs.

Another problem that occurred was statistical errors. For plans with large spot-spacing (distance between each pencil beam spot) and low number of pencil beams, higher statistics were needed. The spot spacing used for a water phantom at CNAO was 2 mm for carbon ions, while for the water phantom used in this project had a spot spacing of 5 - 4 mm. This it might impact the optimization process, as it could be easier for the optimizer to have more spots within the volume to optimize. This is supported by Fjæra et al. [60], which suggests that larger spot spacing may lead to an additional dose outside the PTV for the same optimization problem.

7.2 RBE model dose difference

Comparing the dose distribution from the different optimization strategies, shows that optimizing with a variable RBE-model will give lower physical dose to PTV than for the method which is clinically applied today ($RBE_{1.1}$). The mean physical dose from the WED plan was around 1.60 Gy for all plans, which is 89% of the physical dose from the $RBE_{1.1}$ plan (1.8 Gy). For the UNK and ROR plans, the mean physical dose was around 1.73 Gy which is about 95% of the physical dose from the $RBE_{1.1}$ plan.

Similar results have been produced by Rørvik et al. [61], where considerable differences between RBE and RBE-weighted doses from different RBE models is found. The difference in physical dose distribution is, however, not homogenous in the PTV, as observed, and it is more correct to look at the dose differences in certain areas in the PTV. The general trend for all plans is a higher physical dose difference at the distal end of the beam between the variable RBE plans and $RBE_{1.1}$ plan. In the cubic PTV plan, the physical dose varies 10% from the start of the PTV until the distal end. Grün et al. [62] suggested that the RBE-weighted dose is highest at the distal end of the beam, and could lead to a dose extension. This result is similar to the theoretical water phantom in Appendix B where physical doses from different variable RBE plans also were compared.

The dose difference is, however, more homogenous in the plan with two perpendicular fields, with no larger differences at the distal part of the beam. This might come from that the physical dose from the perpendicular fields evens some of the physical dose distribution out, and is not visible as the field goes into the plane, and therefor leaving the distal part of the beam not visible.

The minimum and maximum doses varies from plan to plan, where the smallest deviation came from the L-PTV plan with two perpendicular fields where it was observed an average minimum and maximum RBE-weighted dose of 1.87 and 2.2 Gy(RBE), respectively. This was expected as it originally provided a good basis for treatment planning with its perpendicular fields. The largest deviation came from the L-PTV plan with angular fields, where it was observed an average minimum and maximum RBE-weighted dose of 1.32 and 2.31 Gy(RBE), respectively. This comes from the unpractical second field which might provide a bad basis for homogenous dose to the PTV.

Overall, there is indication that using RBE-models can give a lower dose overall, reducing risk of side effects while still delivering the same biological dose. The variable RBE models also deviate between themselves, as physical dose from UNK

and ROR is generally higher than WED. This gives rise to the uncertainty that applying variable RBE models in clinical proton therapy might lead to under dosage in the tumor volume. This is also supported by Paganetti et al. [49], which suggests that the clinical RBE of 1.1 is sufficient for now. Finally, the differences suggest that there is lot of uncertainty in the field of RBE models, and more research should be done in this field, before any RBE models is applied clinically.

7.3 Suggestions for further work

After creating a method for optimizing treatment plans with respect to RBE-weighted dose, the possibilities opens up to view physical dose distributions in multiple ROIs, when optimizing with respect to RBE-models. This could provide insight in the effects of RBE-models and help shed a light on the clinical use of RBE models.

Another project would be to implement the optimizer method to the already existing dose verification tool at University of Bergen. The method for using the optimizer is still dependent on manual copy-paste, which should rather be replaced with scripts. This will rule out any potential errors that can occur during this manual process. The script HUchanger.py should also be included in this process, but initially checked for errors and properly verified.

8. Conclusion

In this project, a method for the use of an optimizer together with the FLUKA MC code has been developed and tested on proton therapy treatment plans, applying variable RBE-models. The method is based on an existing tool for reading and translating data from DICOM files, but most scripts are either rewritten or created to match the requirements of the optimizer.

Dose estimates of the optimized plan showed that the method was successful, and provided a good dose conformity for the models used in the different water phantom treatment plans. Promising results were also achieved from a patient plan involving optimization of a single field.

The results showed that the physical dose was reduced, typically on average 6 to 11% from variable RBE models compared to $RBE_{1.1}$. This shows the impact of biological optimization and indicates that the treatment plans optimized with $RBE_{1.1}$ might deliver too high biological dose to the target, in particular in the distal part. Biological optimization could therefore reduce the dose to the healthy tissue in general, and especially to organs at risk located distal to the target.

References

1. Kreftregisteret.no. *Kreftstatistikk*. 2018 [cited 2018 20.4]; Available from: https://www.kreftregisteret.no/Registrene/Kreftstatistikk/.
2. Kogel, M.J.a.A.v.d., *Basic Clinical Radiobiology*, ed. A.V.d.K.a.M. Joiner. 2009: CRC Press.
3. Lederman, M., *The early history of radiotherapy: 1895–1939.* International Journal of Radiation Oncology Biology Physics, 1981. **7**(5): p. 639-648.
4. Thariat, J., *Past, present, and future of radiotherapy for the benefit of patients.* Nat Rev Clin Oncol., 2013. **10**(1): p. 52-60.
5. PTCOG. *Particle Cooperation Group*. 2018 [cited 2018 09.04]; Available from: https://www.ptcog.ch/index.php/facilities-in-operation.
6. Paganetti, H., *Proton therapy physics*. 2012: CRC Press - Taylor & Francis Group.
7. Wilson, R.R., *Radiological Use of Fast Protons.* Radiology, 1946. **47**(5): p. 487-491.
8. C.A. Tobias, J.H.L., J.L. Born et. al., *Pituitary Irradiation with High-Energy Proton Beams: A Prelimenary Report.* Cancer Research, 1958. **18**(2): p. 121-34.
9. Paganetti, H., *Proton Beam Therapy*. 2017.
10. Mohan, R. and D. Grosshans, *Proton therapy - Present and future.* Adv Drug Deliv Rev, 2017. **109**: p. 26-44.
11. Peeters, A., *How costly is particle therapy? Cost analysis of external beam radiotherapy with carbon-ions, protons and photons.* Radiother Oncology, 2010. **95**(1): p. 45-53.
12. Regjeringen. *Statsbudjettet 2018*. 2018 [cited 2018 13.04]; Available from: https://www.statsbudsjettet.no/Statsbudsjettet-2018/Statsbudsjettet-fra-A-til-A/Protonsenter/.
13. Girdhani, S., R. Sachs, and L. Hlatky, *Biological effects of proton radiation: what we know and don't know.* Radiat Res, 2013. **179**(3): p. 257-72.
14. Durante, M., *New challenges in high-energy particle radiobiology.* Br J Radiol, 2014. **87**(1035): p. 20130626.
15. Polster, L., et al., *Extension of TOPAS for the simulation of proton radiation effects considering molecular and cellular endpoints.* Phys Med Biol, 2015. **60**(13): p. 5053-70.
16. Wilkens, J.J. and U. Oelfke, *Optimization of radiobiological effects in intensity modulated proton therapy.* Med Phys, 2005. **32**(2): p. 455-65.
17. Bohlen, T.T., et al., *The FLUKA Code: Developments and Challenges for High Energy and Medical Applications.* Nuclear Data Sheets, 2014. **120**: p. 211-214.
18. Ferrari, A., et al., *FLUKA: A multi-particle transport code (Program version 2005)*. 2005.
19. Mairani, A., et al., *A Monte Carlo-based treatment planning tool for proton therapy.* Phys Med Biol, 2013. **58**(8): p. 2471-90.
20. Rossi, H.H. and M. Zaider, *Microdosimetry and its applications*. 1994.
21. Newhauser, W.D. and R. Zhang, *The physics of proton therapy.* Phys Med Biol, 2015. **60**(8): p. R155-209.
22. Kaderka, R., *Out-of-field dose measurements in radiotherapy*, in *Institut für Festkörperphysik*. 2011, Technische Universität Darmstadt.
23. Bloch, F., *Zur bremsung rasch bewegter teilchen beim durchgang durch materie.* Annalen der physik, 1933. **408**(3): p. 285-320.

24. Bethe, H., *Zur theorie des durchgangs schneller korpuskularstrahlen durch materie.* Annalen der Physik, 1930. **397**(3): p. 325-400.
25. P. Mayles, A.N., and J. C. Rosenwald, eds., *Handbook of radiotherapy Physics: Theory and Practise*. 1st ed. ed. 2007: CRC Press.
26. Janni, J.F., *Energy loss, range, path length, time-of-flight, straggling, multiple scattering, and nuclear interaction probability: In two parts. Part 1. For 63 compounds Part 2. For elements 1 ⩽ Z ⩽ 92.* Atmoic Data and Nulear Data Tables, 1982. **27**(2-3): p. 147-339.
27. ICRP, *The 2007 Recommendations of the International Commission on Radiological Protection. ICRP publication 103.* Ann ICRP, 2007. **37**(2-4): p. 1-332.
28. ICRP, *ICRP Publication 26: Recommendations of the ICRP*. 1977.
29. Burigo, L., et al., *Comparative study of dose distributions and cell survival fractions for 1H, 4He, 12C and 16O beams using Geant4 and Microdosimetric Kinetic model.* Phys Med Biol, 2015. **60**(8): p. 3313-31.
30. Grzanka, L., *Modelling beam transport and biological effectiveness to develop treatment planning for ion beam radiotherapy*, in *The Henryk Niewodnicza«ski Institute of Nuclear Physics*. 2013, Polish Academy of Sciences in Krakow, Poland.
31. Zirkle, R.E., *Exponential and sigmoid survival curves resulting from alpha and X irradiation of aspergillus spores.* Journal of Cellular Physiology, 1952. **39**(1): p. 75-85.
32. Guan, F., et al., *Analysis of the track- and dose-averaged LET and LET spectra in proton therapy using the geant4 Monte Carlo code.* Medical Physics, 2015. **42**(11): p. 6234-6247.
33. Thomas, D.J., *ICRU Report 85—Fundamental Quantities and Units for Ionizing Radiation.* Radiation Protection Dosimetry, 2012. **150**(4): p. 550-552.
34. Herman Cember, T.E.J., *Introduction to Health Physics*. 2009.
35. Roos WP, K.B., *DNA damage-induced cell death by apoptosis.* Trends Mol Med, 2006. **12**(9): p. 440-50.
36. Saha, G.B., *Physics and Radiobiology of Nuclear Medicine*. 2013: Springer.
37. Borges, H.L., *DNA damage-induced cell death.* Cell Res., 2008. **18**(1): p. 17-26.
38. Rossi, A.M.K.a.H.H., *A generalized Formulation of Dual Radiation Action.* Radiation Research, 1978. **75**(3): p. 471-488.
39. Grassberger, C., et al., *Variations in linear energy transfer within clinical proton therapy fields and the potential for biological treatment planning.* Int J Radiat Oncol Biol Phys, 2011. **80**(5): p. 1559-66.
40. Paganetti, H., *Relative biological effectiveness (RBE) values for proton beam therapy. Variations as a function of biological endpoint, dose, and linear energy transfer.* Phys Med Biol, 2014. **59**(22): p. R419-72.
41. Wedenberg, M., *From cell survival to dose response : modeling biological effects in radiation therapy*, in *Dept of Oncology-Pathology*. 2013: Karolinska Institutet.
42. R. G. Dale, B.Jones, *The assessment of RBE effects using the concept of biologically effective dose.* Int. J. Radiat. Oncol, 1999. **43**: p. 639-45.
43. Carabe-Fernandez A, D.R.G.a.J.B., *The incorporation of the concept of minimum RBE (RBEmin) into the linear-quadratic model and the potential for improved radiobiological analysis of high-LET treatments.* Int. J. Radiat. Biol, 2007. **83**: p. 27-39.
44. Rørvik, E., *A phenomenological biological dose model for proton therapy based on linear energy transfer spectra.* Med. Phys., 2017. **44**(6).

45. De Marzi, L., et al., *Treatment Planning Systems and Hadron Therapy Practice in France.* 2017: p. 467-494.
46. Solov'yov, A.V., *Nanoscale Insights into Ion-Beam Cancer Therapy*. 2017.
47. Ytre-Hauge, K.S., *Measurements and Monte Carlo Simulations of Neutron Doses from Radiation Therapy with Photons, Protons and Carbon Ions*, in *Institute of Physics and Technology*. 2013, University of Bergen.
48. Webb, S., *The Physical Basis of IMRT and inverse planning.* The british Journal of Radiology, 2003. **76**(910): p. 678-689.
49. Paganetti, H., et al., *Relative biological effectiveness (RBE) values for proton beam therapy.* Int J Radiat Oncol Biol Phys, 2002. **53**(2): p. 407-21.
50. Unkelbach, J., et al., *Reoptimization of intensity-modulated proton therapy plans based on linear energy transfer.* International Journal of Radiation Oncology*Biology*Physics, 2016.
51. Vlachoudis, V., *FLAIR: a powerful but user friendly graphical interface for FLUKA*. 2009, Proc. Int. Conf. on Mathematics, Computational Methods & Reactor Physics (M&C 2009), Saratoga Springs, New York.
52. W. Schneider, T.B., and W. Schlegel, *Correlation between CT numbers and tissue paramters needed for Monte Carlo simulations of clinical dose distributions.* Physics in Medicine and Biology, 2000. **45**(2).
53. K. Parodi, e.a., *Clinical CT-based calculations of dose and positron emitter distributions in proton therapy using the FLUKA Monte Carlo code.* Physics in Medicine and Biology, 2007. **52**(12).
54. Fedorov A., B.R., Kalpathy-Cramer J., Finet J., Fillion-Robin J-C., Pujol S., Bauer C., Jennings D., Fennessy F.M., Sonka M., Buatti J., Aylward S.R., Miller J.V., Pieper S., Kikinis R, *3D Slicer as an Image Computing Platform for the Quantitative Imaging Network.* Magn Reson Imaging, 2012. **30**(9): p. 1323-41.
55. C. Pinter, A.L., A. Wang, D. Jaffray and G. Fichtinger, *SlicerRT – Radiation therapy research toolkit for 3D Slicer.* Med. Phys., 2012. **39**(10): p. 6332-6338.
56. Fjæra, L.F., *Development of a Monte Carlo based treatment planning verification tool for particle therapy*, in *Department of Physics and Technology*. 2016, University of Bergen.
57. Søbstad, J.M., *Monte Carlo based comparison of constant vs. variable RBE for proton therapy patients*, in *Department of physics and Technology*. 2017, University of Bergen.
58. Wedenberg, M., B.K. Lind, and B. Hårdemark, *A model for the relative biological effectiveness of protons: The tissue specific parameter α/β of photons is a predictor for the sensitivity to LET changes.* Acta Oncologica, 2013. **52**(3): p. 580-588.
59. Wilkens, J.J. and U. Oelfke, *A phenomenological model for the relative biological effectiveness in therapeutic proton beams.* Physics in Medicine and Biology, 2004. **49**(13): p. 2811-2825.
60. Fjæra, L.F. et al., *Linear energy transfer distributions in the brainstem depending on tumour location in intensity-modulated proton therapy of paediatric cancer.* Acta Oncologia, 2017. **56**(6): p. 763-768.
61. Rørvik E. et al., *Exploration and application of phenomenological RBE models for proton therapy* Author sumitted manuscript - PMB-107171, 2018.
62. Grun, R., et al., *Physical and biological factors determining the effective proton range.* Med Phys, 2013. **40**(11): p. 111716.

Appendix A Tables with descriptions belonging to method

In Table A.1, Table A.2 and Table A.3, the description belonging to the different steps in method can be found, with a short description of their role in this project.

Table A.1 Information about the files and scripts for the initial FLUKA simulation.

File/script	Information	Role in master project
Output from TPS	Information about the CT-scans, the regions of interest and the pencil beams are given in DICOM-format	Generally received finished DICOM-files, but helped making one of the plans of one of the phantoms (the L-phantom, described later)
Sort_dicom.py	Converts information from the DICOM-files into FLUKA-input files	Received script, did minor changes
Source.f	Information about beam source	Received script, did minor changes
Fluscw.f	Information about beam weighting	Received script, did minor changes
Input file	Input file for FLUKA	Received script, did minor changes
Voxelfile	Information about the voxels in the phantom	Used standard scripts to create the VOXEL files from the DICOM-files
Information about pencil beam (datfile)	Information about the different parameters for each pencil beam	Output from sort_dicom.py
create_source_and_ Input.py	Script used to modify source and input files	Used this script to make source and input file for each simulation
Split_datfile.py	Script used to modify the datfile and create files for optimizer.	Used this script to make datfile and raster files for each simulation

Table A.2 Overview of files and scripts used for the optimizer and for the FLUKA simulation for dose verification

File/script	Information	Role in master project
Output from HUchanger.py	The script HUchanger.py reads in DICOM files, and gives out information about region of interests (ROIs)	Received script, did minor changes
Information about PTV and ROI	Information about dose and constraints for the different region of interests (ROIs)	Output from HU-changer
Optimizer	C++ based optimizer	Received script. Major part of the master project was to understand how the optimizer worked and how to use it
Information about new weighting	The output from the optimizer, with information about the new weightings of the pencil beams	Used the weighting for dose verification
Make_reopt_datfile.py	Script which changes the weighting from the original plan to the weighting for the optimized plan	Python script made during master project
FLUKA simulation with re-optimized data	Simulation with optimized plan	Put all the scripts together and rand the simulations

Table A.3 Overview of scripts and files used after the dose verification

File/script	Information	Role in master project
Convert_to _dicom.py	Converts the files from the FLUKA simulation into DICOM files	Received script, did minor changes
Plot_1d_results.py	Script which plots the results in 1D	Python script made during master project
Slicer	Software which reads in DICOM-files and provides dose volume histograms (DVHs)	Software
Plot_dicom.py	Plots 2D dose distribution	Received script
DVH	Dose volume histogram (DVH)	Table with dose volume histogram (DVH) provided from Slicer, plotted using python script made for master thesis
2D plot	2D results provided from plot_dicom.py	2D results provided from plot_dicom.py

Appendix B Results from theoretical water phantom

A plan for a water phantom without DICOM-files was also made, where the plan was instead made completely theoretical, where the spot spacing and energy layers were predetermined. The results are given in Figure B.0.1, while a depth dose profile is given in Figure B.0.2.

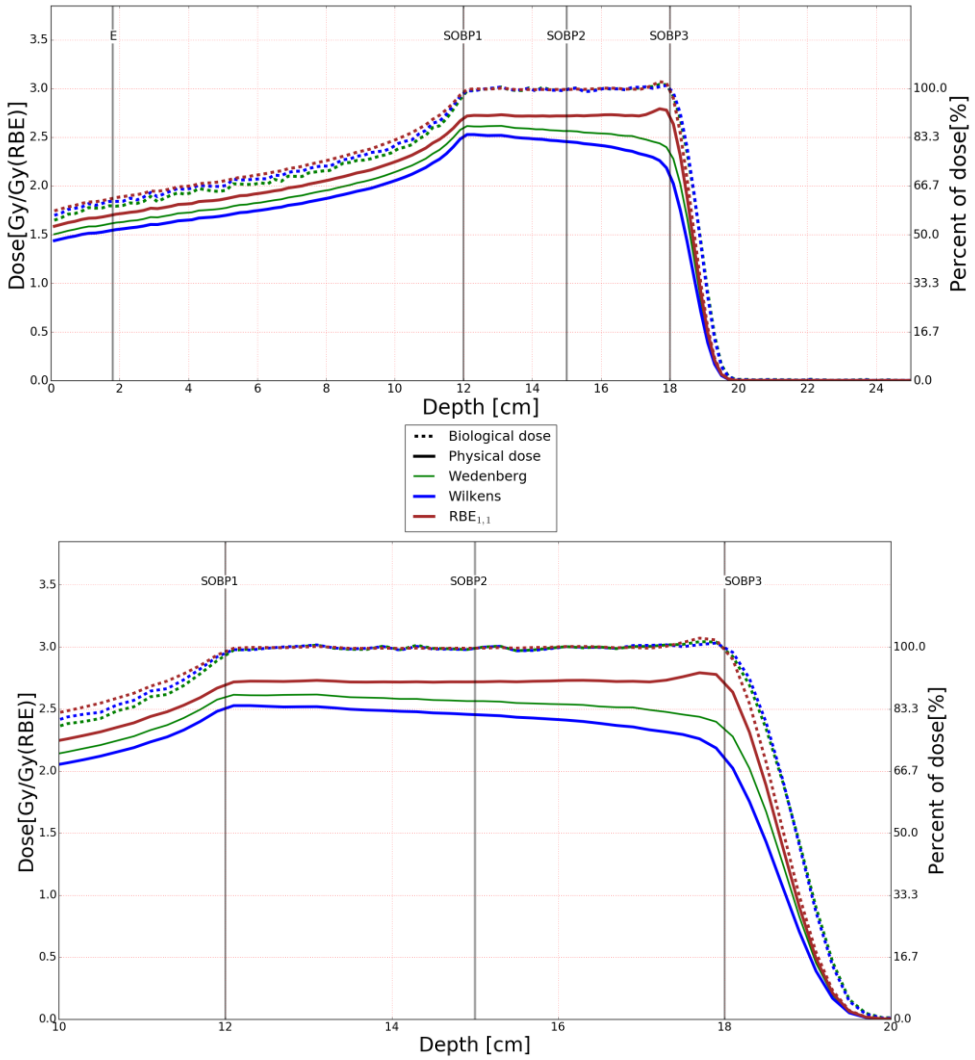

Figure B.0.1 Comparison of physical- (solid lines) and biological dose (dotted lines) distributions for plans optimized with different biological models, for the entire dose profile (above) and zoomed in on the Spread Out Bragg Peak (below).

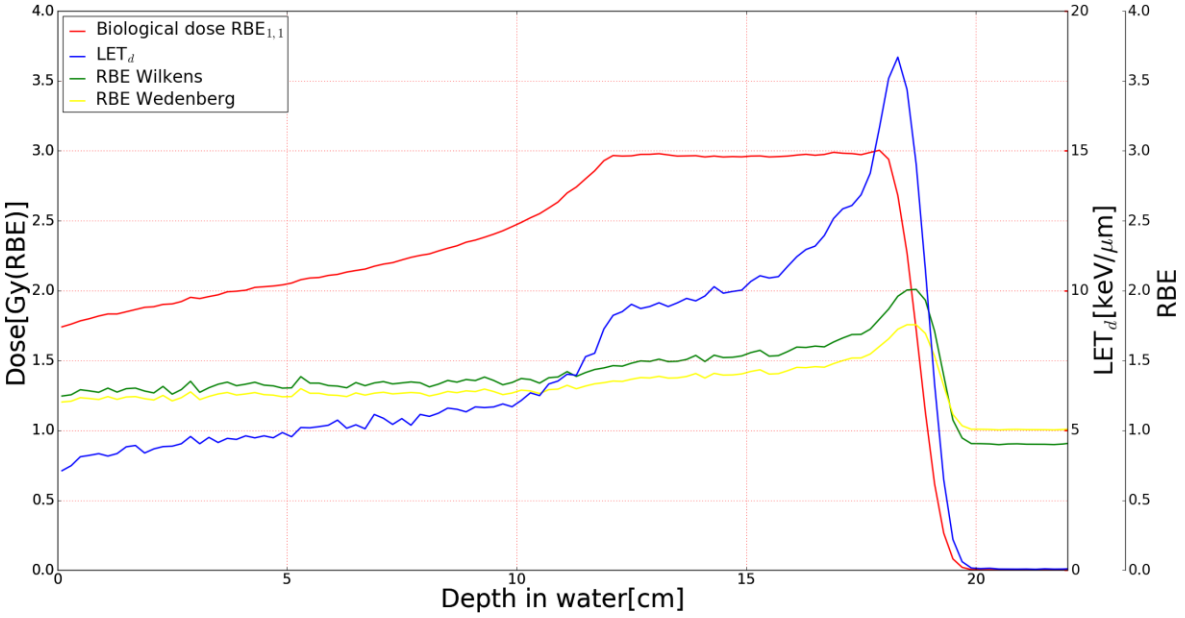

Figure B.0.2 Depth dose for the $RBE_{1.1}$optimized plan plotte together with the LET_d.The RBE for the variable RBE models for the plan is also shown.

Appendix C Extended method for the use of optimizer with protons

Introduction

This document describes in detail how to use the optimizer for proton beams. To summarize the process, first a FLUKA-simulation is ran with the original pencil beam weighting, before running the optimizer. The optimizer will then optimize the weightings of the pencil beams. This result is then used in a second FLUKA simulation to verify the result.

Scripts and properties

This section contains information about the scripts used in the method and how to modify them.

Scripts and files used for first simulation

- Sort_dicoms_for_optimizer.py
  - Modified script for this thesis which creates datfiles with information about the pencil beams. The new pencil beams have no divergence (the angle is constant for all pencil beams), which also only have one direction (z-direction). The directions to use this script are prompted.
- HU-changer.py
  - Script which creates ROI-files for the optimizer. Originally made at CNAO
- create_datfiles.py
  - This script creates chosen number of dat-files with the original pencil beam weighting obtained from TPS. The script has to be modified for each field. This is done at the bottom of the script, where the filename of the original datfile is written, along with the number of desired files.
- create_input_and_source.py
  - This script makes source files and input files for the FLUKA-simulation. It is important the original input file and source file is in the same folder, and since these filenames are read in the script, these names must match as in the bottom of the script. Here, you must change the number of the desired files, also done in the bottom of the script.

    - The input file which is going to be used must also be modified. The number of primary particles must be changed to the desired number of primaries, and all cards for scoring region must be removed, and replaced with the line #include SCORING.flk.
- SCORING.flk
    - Scoring card for the simulation. This script needs to be changed according to gantry angle and patient support angle (it is commented in the script where this has to be done). These angles can be found in the DICOM-files. (use script read_dicom.py, and find the lines labelled gantry angle and patient support angles).
- compile_protons.sh
    - This script compiles executables for the FLUKA-simulation. Modify the first line to match the number of input files that is going to be used. In our simulations the fluscw-routine and source-routine is used.
- proton_run.sh
    - Script to start the FLUKA simulation in the terminal. Before running, it is important to modify the first line to match the number of input files that is going to be used.

Scripts and files used for the optimizer

- do_optimization.sh
    - Starts optimization for the four models: Wedenberg, Unkelbach, Rørvik and RBE = 1.1. It also starts physical optimization. This script starts a number of subscripts, which all needs to be modified. An example of this subscript is 2_proton_biological_optimzation_wed.sh
    - 2_proton_biological_optimzation_wed.sh and other scripts for the different biological models
        - For all these files (labelled with a number in the start of its name), needs to be changed. For a single field a single address line is given at the top. This address needs to the folder with the simulation files (example fort.50). Secondly, make sure the correct PTV is addressed (line labelled –fileroi), and make sure the PTV and OAR files is in the optimizer folder. Check also that the fort-files matches for each model
- create_optimizer_scripts.py
    - Python scripts which makes scripts to run the optimizer with different models and different fields. The first lines in the script represent the choices available. NB, this script makes shell scripts (.sh), and permission to run this script can be denies. The command “chmod u+x filename” must then be run in terminal to obtain the required permissions.

Scripts and files used after the optimization

- create_new_dat_file.py
  - Makes a new datfile with the new weightings from the optimizer. It is important that the two filenames in the bottom of the script matches the file from the optimizer and the file with similar weighting (nyfil_fra_FLUKA_lik_vekting.dat).
- fluscw_IFT.f and source_IFT.f
  - Subroutines used in FLUKA, don't need any changes if the files in the attached folder is used.
- SCORING.flk
  - Scoringcard for the reoptimization process. The volume scored needs to be modified, so the dimensions is similar to the original inputfile.

Procedure

Before use, a folder containing all the files should be made for each field, where the folders must contain the listed scripts:

- create_dat_and_rasterfiles.py
- create_input_and_source.py
- SCORING.flk
- compile_protons.sh
- proton_run.sh
- inputfile
- source.f
- fluscw.f
- optimizer folder labeled "optimizer", containin listed files
  - do_optimization.sh
  - create_optimizer_script.py
  - The optimizer scripts
  - ROIs

This folder will be denoted field_x, which represents each field.

1. FLUKA simulation with equally weighted pencil beams

NB: Before use, the files listed in "Scripts and properties", section needs to be modified according to the directions given above.

The first step is to sort the DICOM files. Open terminal in the folder and write the command:

python sort_dicoms_optimizer.py

To get the original plan, use the script

python sort_dicoms_no_divergence

in a folder containing the same DICOM files. Two folders should have been made now, one containing the files needed for the optimization of the treatment plan, and one folder with the files for the original treatment plan.

Enter the folder containing the files needed for the optimization and copy the dat-files for each field into the folder field_x. In the folder field_x modify the scripts as listed in the start of this document.

The next step is to run the FLUKA simulation. This is done by running the command:

./proton_run.sh

in the terminal. This command compiles the files and starts the FLUKA-simulation.

2. Running the optimizer with the output from the FLUKA simulation

After the initial simulation, the results are given as fortran files belonging to the binning scored e.g. xx_fort.50 if bin 50 is scored. These are going to be read in by the optimizer along with the rasterfiles and region of interest. Enter the optimizerfolder which should lie in the same folder as the results from the initial simulation. Check that all parameters are set in the script create_optimizer_scripts.py and run it

python create_optimizer_scripts.py

This will create the shell scripts for running the optimizer with chosen biological model. If the optimizer has not been run before, the following command lines need to be run:

```
make clean

make RunOptimizer
```

When the optimizer has compiled, the optimization is ran by running the shell script of choosing:

```
./(number_of_model)_proton_biological_optimization_(model_name)_(single_or_multiple_fields).sh
```

The names in the parenthesis represents the options, of models and number of fields, e.g. the use of the Wedenberg model and two fields will therefore be:

```
./2_proton_biological_optimization_wed_two_fields.sh
```

This command will run the optimizer, and folders with the different results will be made.

In these folders, files named pb_xx.res are created from the optimizer, which contains the new information about the pencil beams. Multiple plots are also created including DVHs, which can be used to verify if the optimization process has succeeded, and if the results looks OK. Copy the selected .res file (The final res file is called pb_final.res) into the folder for the FLUKA-simulation with reoptimized result.

3. FLUKA-simulation with results from the optimizer

The res file from the optimizer (e.g. pb_final.res), must first be converted into a format readable for FLUKA. This is done by using the script make_datfile_with_optimized_result.py:

```
python make_datfile_with_optimized_result.py
```

The original datfiles also needs to be included in the folder, and correct filenames needs to be at the end of the script. This script also gives out normalization factors for the field(s).

The files created from this script is named “nyfil_for_reopt_i_fluka_bio.dat” or “nyfil_for_reopt_i_fluka_bio_field_1.dat”, and must be copied into the folder used for the simulation. In the folder for simulation open the inputfile in flair:

flair (inputfile).inp

After opening the input file FLAIR, save it as a new project. Choose number of primaries at the bottom. Then go to compile, and create and executable by clicking on the tab labeled “Executable:”. Save the executable as ex.exe, and add fluscw_IFT.f and source_IFT.f and build with ldpm3qmd. Then run the simulation.

4. Plotting

2D Plot

After the simulation go to tab data and click on process. Then click on files, and data. Choose the bnn-files and click on convert to ASCII. Copy these new files (filename+bnn.lis), into a new folder called BNNLIS. Open a new terminal in the IMPT-folder and run the script

python convert_to_dicom_with_non_1.1.py

The user is prompted for the file locations, which models are going to be used, which BNN files to use and which normalization method to use. For the latter, choose “3 – normalize fields using own factor” and use the normalization factors given earlier to normalize each field

When the new DICOM-files is created use the script

python plot_dicom.py

The user will then be prompted of single or comparison plots, file locations, normalization factors and use scoring outside the PTV. The user will also be prompted of which files to plot and which ROI to view.

Appendix D Plots from output of optimizer

The optimizer provides different plots as output, including cumulative DVHs and slices of the ROIs. The results from L-PTV and cubic PTV are found in Figure D.3 to Figure D.10.

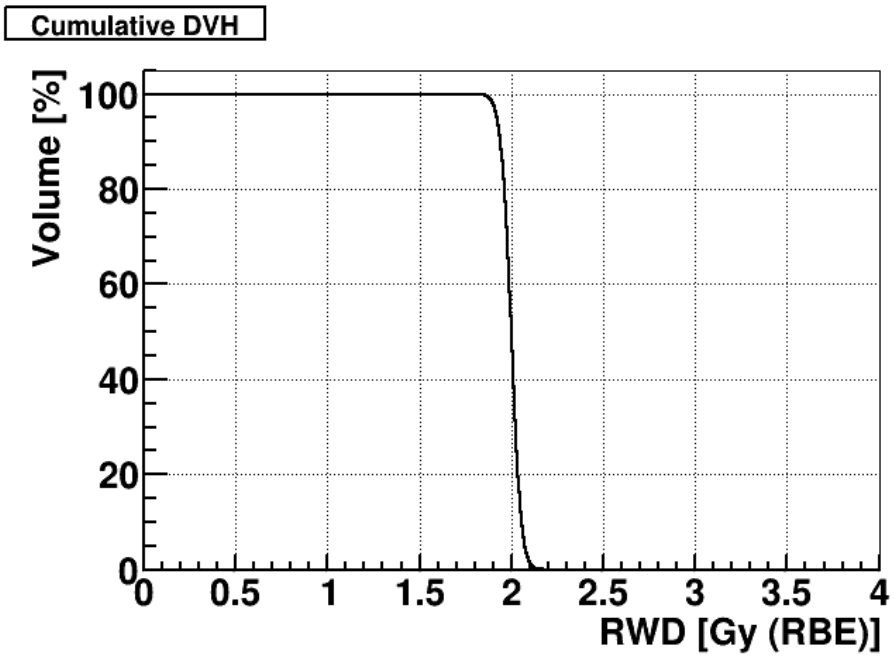

Figure D.3 DVH from the optimizer for plan with the cubic PTV in water phantom.

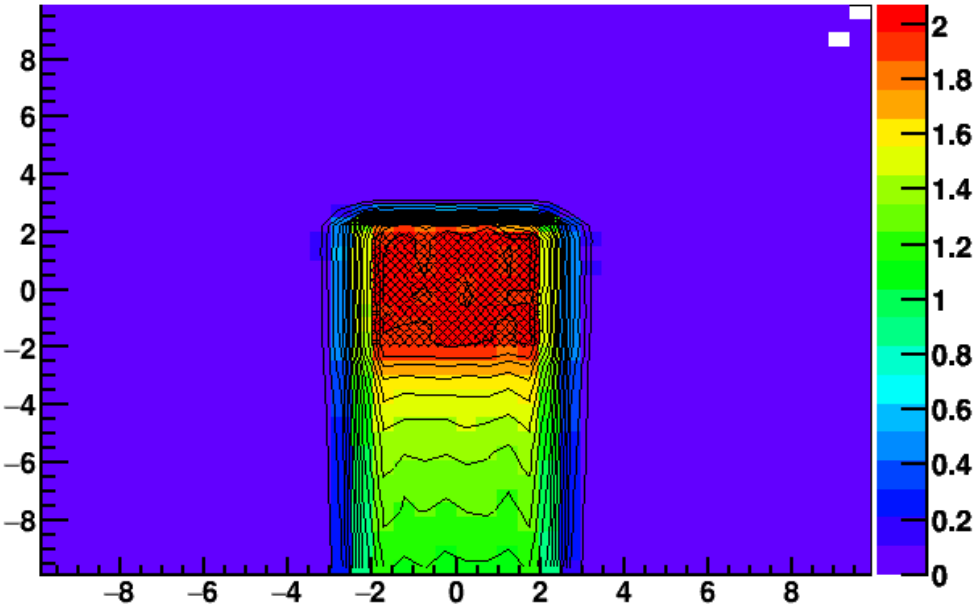

Figure D.4 Slice of the PTV for the cubic PTV plan.

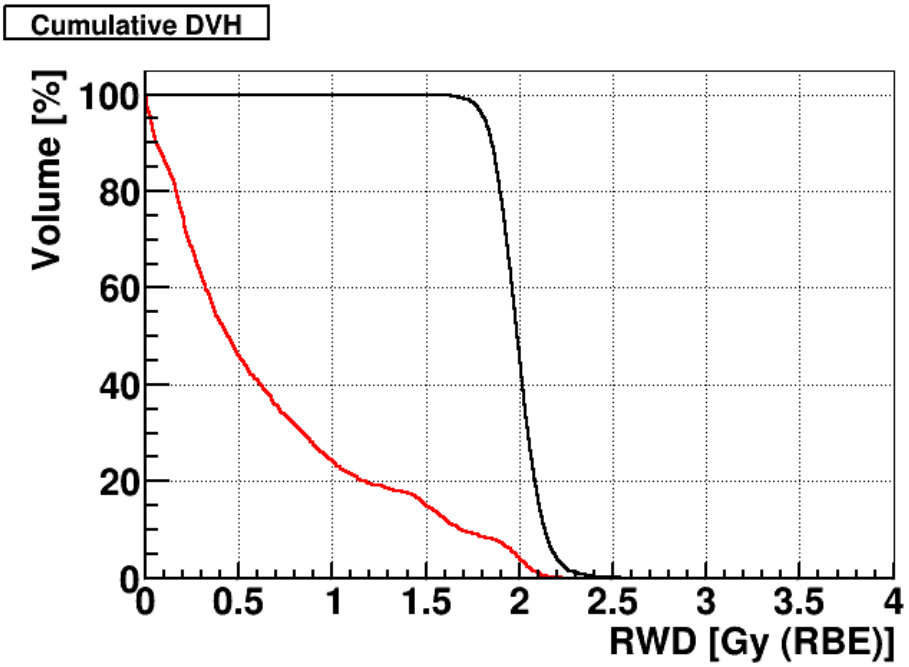

Figure D.5 DVH for plan with L-PTV plan with 1 field. The red line represents the OAR and the black line represents the PTV.

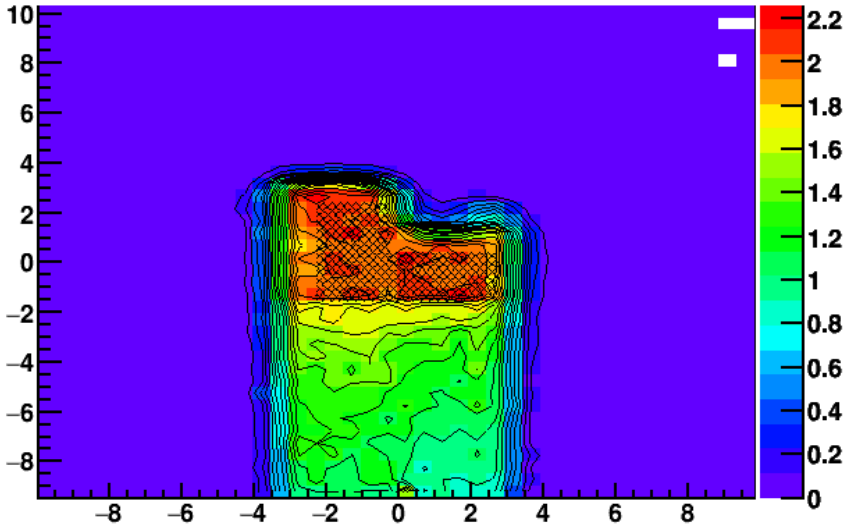

Figure D.6 Slice of the L-PTV in the middle of the water phantom for the L-phantom plan with single field.

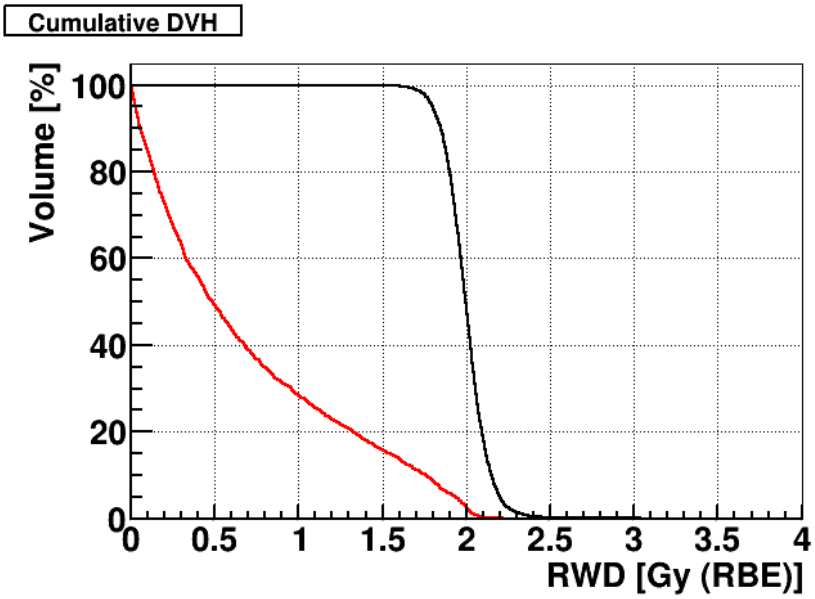

Figure D.7 DVH for L-PTV plan with two perpendicular fields. The red line represents the OAR and the black line represents the PTV.

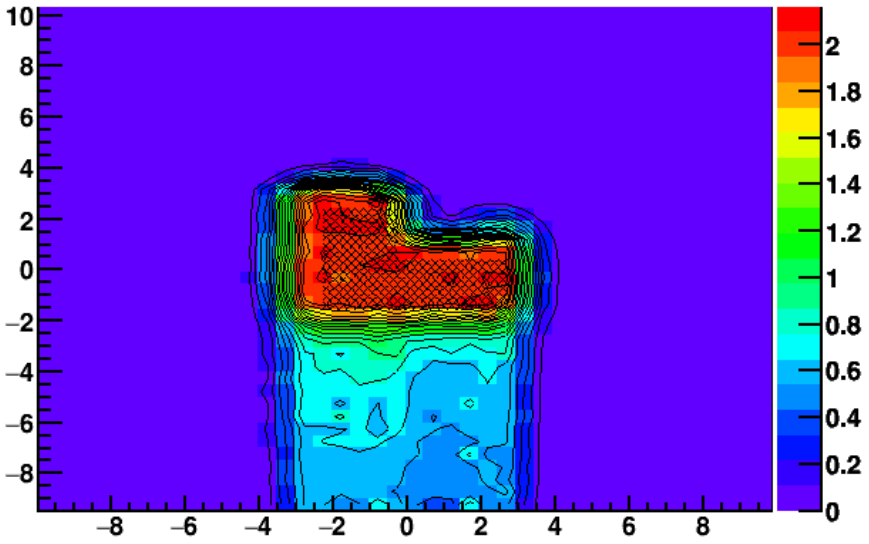

Figure D.8 Slice of the PTV in the L-PTV plan with angular fields.

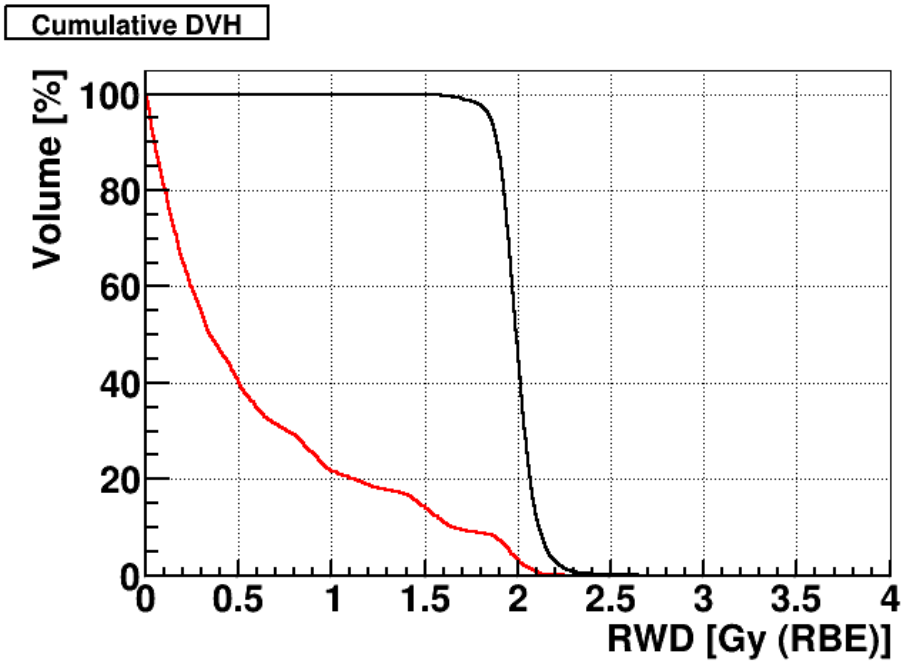

Figure D.9 DVH for the L-PTV plan with angular fields. The red line represents the OAR and the black line represents the PTV.

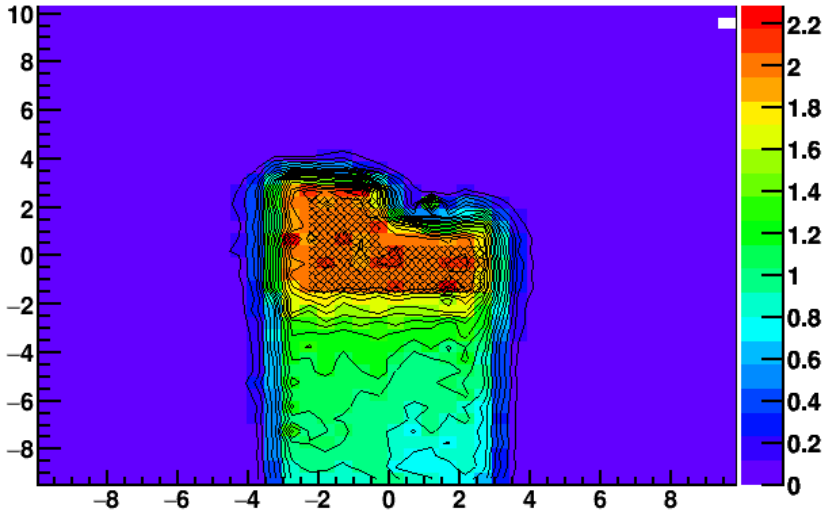

Figure D.10 Slice of the L- PTV in the middle of the water phantom for the plan with perpendicular fields.